Elsevier Editorial System(tm) for Lithos
Manuscript Draft

Manuscript Number:

Title: Multiple pulses, magma mixing and genesis of the giant Allard Lake ilmenite deposit, Quebec

Article Type: Research Paper

Keywords: Grenville; Lac Tio; Titanium ores; Cumulates; Sapphirine

Corresponding Author: Mr. Bernard Charlier,

Corresponding Author's Institution: University of Liège

First Author: Bernard Charlier

Order of Authors: Bernard Charlier; Olivier Namur; Simon Malpas; Cédric de Marneffe; Jean-Clair Duchesne; Jacqueline Vander Auwera; Olivier Bolle

Abstract: The late-Proterozoic Allard Lake ilmenite deposit is located in the Havre-Saint-Pierre anorthosite complex, part of the allochtonous polycyclic belt of the Grenville Province. Presently the world's largest Fe-Ti oxide deposit, it contributes 21% of world ilmenite production with a pre-mining amount in excess of 200 Mt at grades over 60 wt.% hemo-ilmenite. The main ore body is a 10°-dipping ovoid, measuring 1.03 x 1.10 km by 100-300 m-thick. Two smaller bodies are separated by faults and anorthosite. The ore is an ilmenite-rich norite (or ilmenitite) made up of hemo-ilmenite ($Hem_{22.6-29.4}$, 66.2 wt.% on average), andesine plagioclase (An_{45-50}), aluminous spinel and locally orthopyroxene. Whole-rock compositions are controlled by the relative proportion of ilmenite, plagioclase ± orthopyroxene which supports the cumulate origin of the deposit. Ore-forming processes are further constrained by normal and reverse fractionation trends of Cr in cumulus ilmenite that reveal multiple pulses of undifferentiated magma and alternating periods of fractional crystallization and magma mixing. Mixing of magmas produced an hybrid located in the stability field of ilmenite that results in periodic crystallization of ilmenite as the sole liquidus mineral. The absence of correlation between ilmenite composition in adjacent drill-cores favours an emplacement by injection of new batches of magma that carry already crystallized ilmenite crystals. The unsystematic differentiation trends in the Allard Lake deposit, arising from a succession of new magma pulses, hybridisation, and the fractionation of hemo-ilmenite alone or in cotectic plagioclase-hemo-ilmenite cumulates suggest that the deposit was a magma conduit. This dynamic emplacement mechanism associated with continuous accumulation of Fe-Ti oxides and possibly plagioclase buoyancy in a fractionating ferrobasalt explains the formation of the huge concentrations of hemo-ilmenite. The occurrence of sapphirine associated with aluminous spinel and high-alumina orthopyroxene (7.6-9.1 wt.% Al_2O_3) with no plagioclase exsolution supports the role of a retrograde metamorphic overprint during the synchronous Ottawan orogeny, which is also responsible for strong textural equilibration and external granule exsolution of aluminous spinel due to a slow cooling path.

Multiple pulses, magma mixing and genesis of the giant Allard Lake ilmenite deposit, Quebec

Bernard Charlier*, Olivier Namur, Simon Malpas, Cédric de Marneffe, Jean-Clair Duchesne, Jacqueline Vander Auwera, Olivier Bolle

Department of Geology, University of Liège, 4000 Sart Tilman, Belgium

*Corresponding author.
Tel: +32-4-3662250; Fax: +32-4-3662029
E-mail address: b.charlier@ulg.ac.be (B. Charlier).

Submitted to LITHOS

Abstract

The late-Proterozoic Allard Lake ilmenite deposit is located in the Havre-Saint-Pierre anorthosite complex, part of the allochtonous polycyclic belt of the Grenville Province. Presently the world's largest Fe-Ti oxide deposit, it contributes 21% of world ilmenite production with a pre-mining amount in excess of 200 Mt at grades over 60 wt.% hemo-ilmenite. The main ore body is a 10°-dipping ovoid, measuring 1.03 x 1.10 km by 100-300 m-thick. Two smaller bodies are separated by faults and anorthosite. The ore is an ilmenite-rich norite (or ilmenitite) made up of hemo-ilmenite ($Hem_{22.6\text{-}29.4}$, 66.2 wt.% on average), andesine plagioclase ($An_{45\text{-}50}$), aluminous spinel and locally orthopyroxene. Whole-rock compositions are controlled by the relative proportion of ilmenite, plagioclase ± orthopyroxene which supports the cumulate origin of the deposit. Ore-forming processes are further constrained by normal and reverse fractionation trends of Cr in cumulus ilmenite that reveal multiple pulses of undifferentiated magma and alternating periods of fractional crystallization and magma mixing. Mixing of magmas produced an hybrid located in the stability field of ilmenite that results in periodic crystallization of ilmenite as the sole liquidus mineral. The absence of correlation between ilmenite composition in adjacent drill-cores favours an emplacement by injection of new batches of magma that carry already crystallized ilmenite crystals. The unsystematic differentiation trends in the Allard Lake deposit, arising from a succession of new magma pulses, hybridisation, and the fractionation of hemo-ilmenite alone or in cotectic plagioclase-hemo-ilmenite cumulates suggest that the deposit was a magma conduit. This dynamic emplacement mechanism associated with continuous accumulation of Fe-Ti oxides and possibly plagioclase buoyancy in a fractionating ferrobasalt explains the formation of the huge concentrations of hemo-ilmenite. The occurrence of sapphirine associated with aluminous spinel and high-alumina orthopyroxene (7.6-9.1 wt.% Al_2O_3) with no plagioclase exsolution supports the role of a retrograde metamorphic overprint during the synchronous

Ottawan orogeny, which is also responsible for strong textural equilibration and external granule exsolution of aluminous spinel due to a slow cooling path.

Keywords: Grenville; Lac Tio; Titanium ores; Cumulates; Sapphirine

1. Introduction

An ilmenite deposit (50.67°N, 63.67°W) was discovered in June 1946 in the Allard Lake area near a small lake named Lac Tio, by means of the first aeromagnetic survey for ore exploration (Bourret, 1949). It is located 43 km northeast of Havre-Saint-Pierre in Quebec. Following two years of intensive drilling by Kennco Explorations, it has been continuously exploited since 1951 as an open-pit mine. Presently, it is the world's largest hard-rock ilmenite deposit and contributes 21% of world ilmenite production. The hemo-ilmenite ore body has also been intensively studied for its large remanent magnetic anomaly (Hargraves, 1959; Carmichael, 1959; McEnroe et al., 2007).

The Allard Lake ilmenite deposit is situated in the Havre-Saint-Pierre anorthosite complex that is part of the AMCG (Anorthosite-Mangerite-Charnockite-(rapakivi)Granite) suites of the Grenville Province where many occurrences of Fe-Ti-P ores have been described (Dymek and Owens, 2001; Hébert et al., 2005; Morisset et al., submitted). This deposit has usually been considered as an enormous droplet of immiscible Fe-Ti-enriched liquid separated from the residual liquid after the crystallization of the andesine anorthosite (Hammond, 1952; Lister, 1966), a mechanism that has also been proposed for other Fe-Ti deposits (Bateman, 1951; Philpotts, 1967; Kolker, 1982; Force, 1991; Zhou et al., 2005). This model, however, comes up against the inefficiency of an immiscible process to produce monomineralic rocks and evidence for the possible early saturation of Fe-Ti oxides (e.g.

Duchesne, 1999; Charlier et al., 2006; Pang et al., 2008, 2009). Moreover, specific experiments on Fe-Ti magma immiscibility (Lindsley, 2003) have even concluded that Fe-Ti oxide melts do not exist. However, the detailed mechanisms for the formation of huge amount of monomineralic ilmenite ore remain uncertain. Plagioclase buoyancy has been invoked in the Tellnes ilmenite deposit (SW Norway; Charlier et al., 2007) and the Grader layered intrusion (Canada; Charlier et al., 2008) to explain the discrepancy between calculated cotectic proportion of ilmenite (around 15-20 wt.%) and the actual higher proportion of ilmenite in the cumulates. However, in these occurrences, the concentration of ilmenite only ever reaches higher proportions than 50 wt.% locally in thin layers, while the Allard Lake deposit contains more than 100 Mt of ore with > 75 wt.% hemo-ilmenite.

Chemical analyses on new samples from the Allard Lake deposit and an extensive mining database are used in this contribution to understand the crystallization processes that has led to the formation of huge amounts of ilmenite. Complex variations of ilmenite composition in drill-core depth variations are described and evidence the relative role of fractional crystallization, multiple pulses of undifferentiated melts and magma mixing. By analogy with models proposed for the formation of chromitite (Irvine, 1975, 1977), the crystallization of ilmenite as the sole liquidus minerals is discussed. Finally, following a recent estimation of slow cooling rate of the anorthosite and associated rocks (Morisset et al., 2009), we describe postcumulus processes and a metamorphic overprint that substantially modified primary igneous textures and liquidus compositions.

2. Geological setting

The Havre-Saint-Pierre anorthosite complex is part of the late-Mesoproterozoic Grenville Province of North America that extends on 1600 x 350 km along the southeastern margin of the Canadian Shield (e.g. Davidson, 1995, 2008). Rivers et al. (1989) have divided the Grenville Province into three orogen-parallel belts: the parautochtonous belt, the allochthonous polycyclic belt and the allochthonous monocyclic belt. These three belts are limited by two principal boundaries, namely the Grenville Front and the Allochton Boundary Thrust (Fig. 1). The allochthonous belts have also been grouped into different tectonic units on the basis of their Ottawan (1080-1020 Ma; Rivers, 1997) metamorphic signatures (Rivers, 2008). The allochthonous polycyclic belt contains many AMCG suites which have been emplaced in three different pulses, dated around 1160-1140 Ma, 1082-1050 Ma and 1020-1010 Ma (Higgins and van Breemen, 1996; Corrigan and van Breemen, 1997). The Grenvillian orogenic belt of Laurentia is correlated with the Sveconorwegian orogenic belt of the Baltic shield (Rivers et al., 1989; Romer, 1996; Rivers and Corrigan, 2000).

Among the AMCG suites, the composite Havre-Saint-Pierre anorthosite crops out along the lower northern shore of the Saint Lawrence estuary. It covers an area of 20.000 km^2 and is made up of several anorthositic lobes separated by monzonitic, mangeritic to charnockitic envelopes (Fig. 2; Wodicka et al., 2003). The Allard Lake anorthosite, in which the ilmenite deposit was emplaced, has been dated at ca. 1061 Ma (U-Pb on zircon; Morisset et al., 2009), which is the same age as that of the small neighbouring Rivière au Tonnerre anorthosite, dated at 1062 ± 4 Ma (U-Pb on zircon; van Breemen and Higgins, 1993). These ages are coeval with the second stage of the Grenville metamorphism of the Ottawan orogeny (1080-1020 Ma; Rivers, 1997, 2008; Rivers et al., 2002). Dating of the mangeritic envelope of the Allard anorthosite from the Magpie river area gives an older age of 1126 +7/-6 Ma (U-Pb on zircon; Emslie and Hunt, 1990). The Havre-Saint-Pierre complex is probably correlated with other anorthositic suites of Chateau-Richer, St-Urbain, Mattawa and Labrieville (Fig. 1; Owens et al., 1994; Owens and Dymek, 2001, 2005; Morisset et al. 2009).

The Allard anorthosite displays a dome structure surrounded by a continuous jotunitic to mangeritic margin of 1-10 km (Hocq, 1982). Rocks display microscope evidence of ductile deformation (undulatory extinction of plagioclase) and dynamic recrystallization. Lithologies are essentially constituted by coarse-grained hololeucocratic andesine anorthosite with plagioclase An_{37-49}, Or_{3-7}, 1000-1200 ppm Sr and 200-500 ppm Ba (Hargraves, 1962; Dymek, 2001) that contains less than 5% of orthopyroxene, ilmenite ± clinopyroxene. Rocks may be equigranular (ca. 5 mm-2 cm) but some rocks contain large plagioclase phenocrysts of 20 cm long. Norites and even leuconorites are rare and represent less than 1% of the outcropping surface. Sheets and layers of oxide-rich (gabbro-)norites are common (Hargraves, 1962). Enclaves of labradoritic anorthosites (An_{66-74}, 350-550 ppm Sr, <50-100 ppm Ba) occur in the western part of the anorthosite (Hocq, 1982; Dymek, 2001). Olivine has been described in labradoritic gabbros (Hocq, 1982) and garnet-bearing anorthosites occur at the west of the Magpie lake (Sharma and Franconi, 1975). All these characteristics together with the local occurrence of high-alumina orthopyroxene are typical features of massif-types anorthosites emplaced through polybaric crystallization (Emslie, 1985; Charlier et al., submitted).

3. Sampling and analytical methods

An extensive mining database of 172643 samples from 236 drill-cores has been used to draw the morphology of the deposit. The density (g/cm^3) of these samples has been determined by weighing the dry sample in air and then in water, following Archimedes' principle. Among these samples, 3923 rocks have been analysed for whole-rock composition by the mining company using XRF method. Each sample represents a 3 m portion of a split drill core. A few samples represent shorter sections (1-2 m). Seven cores have been selected for detailed discussion and are reported in Fig. 3. New samples were also collected along 3 cores (labelled T873; T875 and N10) and fifteen samples have been selected in the open-pit (Fig. 3).

Ilmenite concentrates (60-150 µm), using heavy liquids (bromoform and Clerici's solution) and a Frantz isodynamic magnetic separator, were analysed for major elements (Si, Ti, Al, Fe, Mn, Mg) by XRF on lithium-borate fused glass, and for trace elements (V, Cr, Zn, Zr, Nb) on pressed powder pellets following the method of Duchesne and Bologne (2009). Plagioclase grains (60-150 µm), separated by using flotation in bromoform and magnetic separation, were analysed for major elements by XRF on lithium-borate fused glass and for Sr and Ba by XRF on pressed powder pellets.

Microprobe analyses of orthopyroxene and aluminous spinel were performed using the CAMECA SX50 of the Bochum University (Germany). An accelerating voltage of 15 kV and a beam current of 15 nA were used. Chemical analyses were corrected with the ZAF software. The following standards were used: pyrope for Mg and Al; andradite for Si, Fe and Ca; spessartine for Al and Mn; rutile for Ti; jadeite for Na; ZnO for Zn; Cr_2O_3 for Cr and V metal for V.

4. Morphology and petrography of the deposit

The Allard Lake ore body may be subdivided into three different units (Fig. 3), namely the Main Deposit, Cliff and North-West. The main deposit has a oval outcrop measuring 1100 x 1030 m. The thickness ranges from 100 to 300 m and the ore body is dipping 10-15° to the east. The remaining tonnage is estimated at 125 Mt with an estimated 120 Mt already mined. The Cliff ore body has an ellipsoidal shape in map view and lies along the west side of the main body from which it is separated by anorthosite. The contacts at the base of the ore body with the host anorthosite is sharp and undulating. The Cliff ore reserves are estimated at 8.4 Mt. The North-West ore body is a 100 to 60 m-thick layer, representing 5 Mt of ore reserve.

The ore is a coarse-grained (5-20 mm) ilmenite-rich norite or ilmenitite, essentially made of tabular crystals of hemo-ilmenite (66.2 wt.% on average) and plagioclase.

Histograms of the distribution of ilmenite proportions show that 50% of the samples contain more than 76.3 wt.% (Fig. 4). Samples with less than 65 wt.% ilmenite are equally represented. This is much more than the Tellnes ilmenite deposit (40 wt.% ilmenite on average; Charlier et al., 2006). Typical accessory minerals include aluminous spinel, orthopyroxene and Ti-phlogopite. Minor amounts of disseminated sulfides (pyrite, pyrrhotite, chalcopyrite, millerite and Co-Ni sulfides) are present. Primary magnetite is absent in the ore; the most common magnetite is secondary in origin and together with rutile and anatase results from late-stage alteration of hemo-ilmenite. Calcite and gypsum occur locally as alteration products in veinlets.

Several groups of rocks have been distinguished among the samples based on the presence and relative proportions of plagioclase, ilmenite and orthopyroxene: anorthosite (>90% plagioclase; Fig. 5a-b), ilmenite-norite (<90% plagioclase, ilmenite), norite (<90% plagioclase, ilmenite, >2% orthopyroxene; Fig. 5c), opx-ilmenitite (>70% ilmenite, plagioclase, >2% orthopyroxene) and ilmenitite (>70% ilmenite, plagioclase; Fig. 5d). Two types of anorthosite occur: the host Havre-Saint-Pierre anorthosite and anorthositic layers and lenticular beds in the massive ore. Both types are petrographically very similar and only distinguished on their location. Norites occur in association with both types of anorthosites.

In the Allard deposit, ilmenite grains display 120° triple junctions (Fig. 5d) typical of an annealing texture resulting from static recrystallization. They contain two generations of lenses of exsolved hematite with less than 50% hematite exsolution and are thus referred to as hemo-ilmenite (Fig. 5e). Exsolved hematite from grain to grain commonly display a preferred orientation, implying that the lattice of ilmenite grains had a similar orientation before the exsolution process. Twinning in ilmenite and equant ilmenite grains included in plagioclase are locally observed. Ilmenite may be rimmed by a thin zircon corona (Fig. 5f; Morisset and Scoates, 2008) and baddeleyite locally occur as small euhedral grains included in ilmenite.

Hemo-ilmenite microstructures and the implications for magnetic properties are detailed in McEnroe et al. (2007).

Large grains of aluminous spinel are present at the margin of ilmenite crystals and are interpreted as representing external granule exsolution. Aluminous spinel also occurs as exsolved lenses or small granules in ilmenite. A noticeable decrease in the amount of hematite lamellae in ilmenite is observed close to the exsolved aluminous spinel (Fig. 5e) which implies a subsolidus reaction.

Prismatic orthopyroxene (1-4 mm) occurs in a few samples. It commonly contains Schiller lamellae (hemo-ilmenite) and may include ilmenite grains (Fig. 6a). Rare symplectitic intergrowths of orthopyroxene and aluminous spinel have been detected (Fig. 6b). Sapphirine has been observed in three thin sections out of a hundred (Fig. 6c-d) and is usually in contact with orthopyroxene and aluminous spinel. Clinopyroxene, locally containing small core of orthopyroxene, is the main Fe-Mg silicate in anorthosites.

5. Mineral chemistry

5.1. Ilmenite

Separated ilmenites have been analysed for major and some trace elements (Table 1). The hematite content varies between $Hem_{22.6}$ and $Hem_{29.4}$. Cr ranges from 450 to 2277 ppm and has a poor positive correlation with V (1793-2365 ppm) (see later in Fig. 13). MgO (1.59-3.22 wt.%) is positively correlated with Al_2O_3 (0.36-1.95 wt.%) and Zn (27-218 ppm). This is interpreted to result from variable spinel content in ilmenite and/or from separation of spinel from ilmenite during the mineral separation process. Zr in ilmenite span a large range from 22 to 1261 ppm. This is most probably related to the amount of zircon exsolved from ilmenite.

Ilmenite composition displays irregular patterns with drill-core depth variations (Fig. 7). The trends in each drill-cores are characterized by abrupt shifts for all the elements. Both normal trends (decreasing content of compatible elements with decreasing depth) and reverse trends (increasing content of compatible elements with decreasing depth) are observed.

5.2. Plagioclase

The range of plagioclase compositions in the Allard Lake deposit and in the surrounding Allard anorthosite is clearly andesinic (Fig. 8; Table 2). Plagioclase compositions in the ilmenite deposit vary from $An_{50.6}$ to $An_{41.7}$ and $Or_{0.4}$ to $Or_{6.5}$. Sr varies from 851 to 1518 ppm and Ba, from 101 to 461 ppm. These compositions are close to the plagioclase composition in the Havre-Saint-Pierre anorthosite: $An_{49.0\text{-}45.4}$, $Or_{3.6\text{-}7.1}$, Sr 962-1212 ppm and Ba 196-437 ppm. Moreover, anorthositic rocks in the Allard deposit display a similar range: $An_{51.0\text{-}43.7}$, $Or_{6.3\text{-}5.1}$, Sr 1111-1165 ppm and Ba 194-398 ppm, and thus cannot be distinguished from plagioclase of the host Havre-Saint-Pierre anorthosite.

Histograms of the distribution of plagioclase composition for each petrographic type (Fig. 8) show that plagioclase in ilmenitite and opx-ilmenitite (ilmenite-rich rocks) have a significant lower Or content compared to plagioclase from anorthosite and norite (plagioclase-rich rocks).

5.3. Aluminous spinel

Average compositions for aluminous spinel have X_{spinel} ranging from 0.564 to 0.628 (Table 3). The MnO content is low (0.05-0.06 wt.%) while the ZnO content is relatively high from 1.12 to 2.02 wt.% ($X_{gahnite}$ = 0.020-0.038). Detailed profiles across spinel grains reveal significant zonings (Fig. 9), particularly for Mg/Fe proportions and for the Cr_2O_3 content. Single grains have a higher $X_{hercynite}$ and lower Cr_2O_3 contents in the core and X_{spinel} and Cr_2O_3 enrichments towards the margin. ZnO is also higher at the margin while no systematic variations for the MnO content have been observed.

5.4. Pyroxenes

The composition of orthopyroxene ranges from $Ens_{75.7}$ to $Ens_{58.4}$ (Table 4). The Al_2O_3 content of orthopyroxene spans a wide range from 1.48 to 9.08 wt. % and two groups may be distinguished: low-alumina (1.48-3.09 wt.%) and high-Wo (0.6-1.5 mol%) orthopyroxenes on one hand and high-alumina (7.62-9.08 wt.%) and low-Wo (0.1-0.3 mol%) orthopyroxenes on the other hand. The latter group of orthopyroxene occurs in samples in which sapphirine was detected. Contrarily to high-alumina orthopryxene megacrysts (Emslie, 1975; Longhi et al., 1993; Charlier et al., submitted) interpreted to have crystallized under high pressure (11-13 kbar), Al-rich orthopyroxene from the Allard deposit does not contain plagioclase exsolutions. MnO (0.17-0.84 wt.%) has a clear negative correlation with Mg# (Fig. 10). The Mg# of clinopyroxene ranges from 77.6 to 72.9 (Table 4).

5.5. Sapphirine

Sapphirine composition has been recalculated according to the scheme of Owen & Greenough (1991). The analysed sapphirines are markedly magnesian ($Mg/(Mg+Fe^{2+})=0.83$). The calculated $Fe^{3+}/(Fe^{2+}+Fe^{3+})$ ratios are 0.33-0.35. Cr_2O_3 has not been analysed but reach 0.50 wt.% in similar occurrences (Morisset et al., submitted).

6. Whole-rock composition

Whole-rock analyses are plotted in major element binary diagrams (Fig. 11). TiO_2 and Al_2O_3 have been chosen as the variation index, as they are essentially correlated with the modal abundance of ilmenite and plagioclase, respectively. Compositional ranges of plagioclase, ilmenite and the two groups of orthopyroxene are also plotted.

Whole-rock compositions display a large range: TiO_2 0.61-41.71 wt.%; Fe_2O_{3tot} 0-66.30 wt.%; Al_2O_3 0-26.23 wt.%; CaO 0-10.33 wt.%; MgO 0.01-7.48 wt.%. It is obvious that the bulk composition is essentially controlled by the relative proportion of ilmenite and plagioclase as demonstrated by a linear trend between ilmenite and plagioclase composition in a TiO_2 vs. Al_2O_3 diagram (Fig. 11). When MgO is plotted as a function of Al_2O_3 or TiO_2, a minority of samples define a trend to orthopyroxene composition. Anecdotally, some samples display a significant CaO-enrichment (CaO vs. Al_2O_3 diagram; Fig. 11) which is related to the presence of late calcite and gypsum veins in some rocks.

7. Discussion

7.1. Evidence for magma mixing

Because of the high value of D_{Cr}^{Ilm} (e.g. Klemme et al., 2006), the Cr content of ilmenite is a good indicator of primitive magma replenishment, since it should abruptly increase after a new injection of undifferentiated melt. Although major and trace element compositions of whole-rocks reflect the modal mineralogy of the samples, the Cr/TiO_2 ratio may be considered as a proxy for the Cr content of the ilmenite, because Cr is exclusively contained in ilmenite and aluminous spinel that result from exsolution from ilmenite. Using the average TiO_2 content of ilmenite (37.71 ± 0.75 wt.%; Table 1), the Cr content of ilmenite (Cr_{ilm}) may be calculated from whole-rock composition (Cr_{WR}) using the equation:

$Cr_{ilm}=Cr_{WR}* TiO_{2ilm} / TiO_{2WR}$

In accordance with the measured composition of ilmenite (Fig. 7), the calculated Cr concentration of ilmenite in 8 drill-cores also display large variations (Fig. 12). Normal (decreasing Cr content) and reverse (increasing Cr content) trends alternate at a scale lower than 10 m, which implies crystallization of ilmenite from continuously changing melt composition as a result of three processes: (1) crystal fractionation (normal trends), (2) new primitive magma emplacement and (3) progressive magma hybridisation. Even if the shifts to more primitive compositions are locally abrupt, which suggests crystallization of ilmenite from a new undifferentiated melt composition (possibly without mixing), many reverse trends are outlined by a sequence of samples that become Cr-richer, which implies progressive hybridisation of the melt.

It is also noticeable that no correlation can be done between drill-cores that are spatially very close (e.g. Ti05-14, T39 and AC-25 which are less than 100 m away; Fig. 12). This might favour an emplacement by injection of new batches of magma carrying already crystallized ilmenite crystals, a mechanism similar to that proposed by Mondal and Mathez (2007) for the formation of UG2 chromitite layer in the Bushveld Complex. This mechanism is not incompatible with the crystallization of ilmenite from a magma that become progressively more primitive due to mixing with undifferentiated magma.

7.2. Magma mixing and ilmenite stability: a view from chromitites

Magma mixing producing a hybrid located in the stability field of chromite, which becomes the only liquidus mineral, has been proposed to explain the origin of chromitite layers in magma chambers (Irvine, 1975, 1977). Mixing occurs either between the resident fractionated magma and a new primitive one, or by contamination of the resident magma by a siliceous component. This mechanism has been corroborated by many other studies (e.g. Roeder and Reynolds, 1991; Campbell and Murck, 1993; Kinnaird et al., 2002) that have provided supporting evidence from mineral compositions, modal proportions, fluid dynamics, experimental studies and isotopic ratios.

Cotectic crystallization of chromite with olivine (or orthopyroxene) associated with gravitational sorting has been excluded on the basis of textural relationships and because of inconsistencies with the Cr budget (Eales and Reynolds, 1986). Indeed, the cotectic proportion of chromite and olivine can vary because of the curved-shape of the olivine-chromite cotectic but remains lower than 2:98 (Irvine, 1977). Consequently, the counterpart olivine cumulate pile would be at least 50 m thick for a chromitite layer 1 m thick, a proportion which is not observed. Moreover, because of the low solubility of Cr in basic magma (ca. 1000 ppm; Barnes, 1986; Murck and Campbell, 1986), the required liquid thickness of the parental liquid would be unrealistically high. Mass balance considerations thus require that chromite was the only liquidus mineral, at least for a while.

Phase diagrams for plagioclase-ilmenite saturated liquids are poorly constrained. Nevertheless, plagioclase and ilmenite are known to crystallize as the first liquidus phases in several intrusion: Bjerkreim-Sokndal (SW Norway) and Grader layered intrusions (Wilson et al, 1996; Charlier et al., 2008) and the Tellnes ilmenite deposit (Charlier et al., 2006) are the most obvious examples. Calculations of the cotectic proportions of ilmenite in ferrobasalts led to values of 17.5 wt.% in the Tellnes ilmenite deposit (SW Norway; Charlier et al., 2007) and to 21 wt.% in the Grader layered intrusion (Charlier et al., 2008). These values, in accordance with experimental works on ferrobasalts (Toplis and Carroll, 1995), are low compared to the modal proportions observed in these two intrusions. However, the presented arguments against magma mixing and in favour of continuous fractional crystallization are based on the continuous and systematic cryptic layering of cumulus phases, successfully modelled by simple Rayleigh fractionation. Thus, the invoked mechanism for ilmenite enrichment was thus simply flotation of plagioclase.

In the Allard Lake deposit, even if ilmenite enrichment due to plagioclase flotation cannot be ruled out, it is evident that it is not solely associated with continuous fractional crystallization. As previously discussed, magma mixing is evidenced by reverse trends (Fig. 12). This is also shown in Fig. 13, where the evolution of Cr in ilmenite as a function of V does not display a single trend. Ilmenite compositions are spread between two differentiation trends: fractionation of pure ilmenite and of a plagioclase-ilmenite cotectic proportion. Two plausible cotectic fraction of ilmenite (X_{ilm} = 0.21 and 0.16) are displayed, in accordance with the range of values calculated from natural and experimental works (Toplis and Carroll, 1995; Charlier et al., 2007, 2008). It is highly probable that the plagioclase-ilmenite cotectic is curved and that mixing of two magmas lying on the cotectic will produce an hybrid located in the stability field of ilmenite, that will crystallize alone until the liquid joins the cotectic. However, the paucity of rocks with cotectic proportions of ilmenite and plagioclase (15-25 wt.% ilmenite and 85-75 wt.% plagioclase) leads to suggest that the liquid did not follow the cotectic during significant periods of fractionation, in accordance with the multiple magma mixing events recorded by ilmenite compositions. Moreover, further ilmenite enrichment might also result from plagioclase flotation, even if no direct evidence of plagioclase accumulation at the top of the intrusion has been observed. Plagioclase from the Allard Lake ilmenite deposit has the same composition than the plagioclase from host Havre-Saint-Pierre anorthosite. Thus the floated cumulates would be indistinguishable from the enclosing anorthosite.

7.3. Conduit or layered intrusion?

The Allard Lake deposit occurs as a huge mass of massive ilmenite, with minor norites. Some layering occurs close to the margin with the host anorthosite, but these layers cannot be traced along significant distances. Lateral correlations of the composition of ilmenite, i.e. same Cr content in ilmenite and similar evolutional trends with drill-cores depth, are impossible even where an orientation plane is revealed by the occurrence of fine anorthosite layers. These unsystematic stratigraphical variations contrast with the Grader layered intrusion that displays continuous evolution of liquidus phase compositions and a sandwich horizon where the upper and lower solidification fronts met (Charlier et al., 2008).

The occurrence of multiple magma mixing events further supports the view that the Allard Lake deposit should not be regarded as a slowly cooled magma chamber but rather as a magma conduit in which ilmenite accumulates. We moreover suggest that the Allard Lake deposit might also be the conduit system of the 4-5 km diameter Grader layered intrusion, which is situated less than 2 km away from the Allard Lake mine. The base of Grader is highly similar to the Allard Lake deposit with a disturbed Cr evolution in ilmenite in its 25 m-thick basal massive ilmenite-rich portion (Charlier et al., 2008). There, ilmenite contains 800-900 ppm Cr and is more evolved compared to primitive ilmenite in Allard Lake (ca. 2400 ppm Cr), but corresponds to the most abundant values of the deposit (Fig. 14). The Grader layered intrusion reaches more evolved composition with apatite, magnetite and clinopyroxene as liquidus phases, not observed in the Allard Lake deposit.

Such a dynamic environment of emplacement has also been documented for major Ni-Cu sulfide deposits such as Noril'sk, Jinchuan and Voisey's Bay (e.g. Li and Naldrett, 1999; Maier et al., 2001; De Waal et al., 2004; Li et al., 2004). In the Allard Lake deposit, the potential for ilmenite ore formation in a conduit system is enhanced by the injection of multiple pulses of undifferentiated magma that may crystallize large amount of ilmenite. This mechanism is also convenient to explain the absence of evolved cumulates or residual liquids.

7.4. Postcumulus processes and metamorphic overprint

The Allard anorthosite has been dated at ca. 1061 Ma (U-Pb on zircon; Morisset et al., 2009), which is synchronous with the second stage of the Grenville metamorphism of the Ottawan orogeny (1080-1020 Ma; Rivers, 1997, 2008; Rivers et al., 2002). Moreover, U-Pb dating on metamorphic minerals from the Havre-Saint-Pierre complex reveals a metamorphic phase around 1062 Ma and monazites in paragneiss have been dated between 1063 and 1047 Ma (Wodicka et al., 2003). The similarity of the ages for the crystallization of the Havre-Saint-Pierre anorthosite and the Ottawan metamorphic peak is consistent with the very low cooling rates estimated for the anorthosite (3-4°C/m.y.r.; Morisset et al., 2009). Based on their Ottawan metamorphic signature, the tectonic unit that includes the Havre-Saint-Pierre anorthosite complex has been included in the allochtonous medium-low pressure belt of the Grenville orogen, characterized by penetrative metamorphism under a relatively high geothermal gradient followed by slow cooling (Rivers, 2008).

During the slow cooling of the Havre-Saint-Pierre anorthosite complex, textural equilibration of the Allard ore has occurred and ilmenite has recrystallized as coarse polygonal grains. This example of textural coarsening (e.g. Higgins, 1993) is supported by the smaller size of ilmenite grains when included in silicates and preserved from recrystallization. Aluminous spinel has also exsolved and migrated to grains boundaries during recrystallization to form large external granules. These exsolutions have continued reequilibrating with adjacent ilmenite grain, as shown by the zoning of aluminous spinel grain that have Fe-rich cores and Mg-rich rims (Fig. 9).

Moreover, in the Allard Lake deposit, two types of orthopyroxene have been described: (1) primary magmatic low-alumina orthopyroxene, common in the anorthosite and some ores, and (2) high-alumina orthopyroxene always associated with sapphirine and spinel, detected only in a few samples. Sapphirine-bearing rocks in the Havre-Saint-Pierre anorthosite have also been described in an ilmenite-rich dyke close to the Big Island lake (Bergeron, 1986; Morisset et al., submitted). These rocks also contains large amount of rutile (up to 15 wt.%) some spinel and corundum. The sapphirine-rutile-ilmenite rocks of the Havre-Saint-Pierre anorthosite are similar to those described in the St-Urbain anorthosite (Warren, 1912; Dymek, 1984; Morisset et al., submitted). High-alumina orthopyroxene and sapphirine are interpreted as resulting from subsolidus reaction during slow cooling of low-alumina orthopyroxene with spinel previously exsolved from ilmenite.

8. Conclusions

The genesis of world-class deposits including Fe-Ti oxide ore deposits is a combination of particular processes that give rise to unique economic concentrations of ore-minerals. Although the petrogenesis and emplacement of massif-type anorthosites that host Fe-Ti oxide ore deposits have been investigated for decades, the early saturation of ilmenite in andesine anorthosite (after plagioclase and before ferromagnesian silicates) has only been recognized recently. While immiscibility was experimentally discarded to produce pure ilmenite ore (Lindsley, 2003), early saturation of ilmenite associated with plagioclase flotation in a dense ferrobasaltic melt, such as in the Tellnes deposit (Charlier et al., 2007), is nevertheless not sufficient to explain the formation of the huge amount of massive ilmenite in the Allard Lake deposit. Our new data on ilmenite and whole-rock compositions from this deposit that are presented here demonstrate intermittent crystallization of ilmenite as the unique liquidus phase and its accumulation in a conduit system. The crystallization of ilmenite alone results from magma mixing that produces hybrid melts located in the stability field of ilmenite. These processes satisfactorily explain the geochemical features of the Allard deposit: small scale normal and reverse trends of compatible element as well as lack of lateral correlations for ilmenite composition.

Acknowledgements

Rio Tinto Iron and Titanium is gratefully acknowledged for permission to access to the database and to publish the new data. Martin Sauvé and Tommy are thanked for their assistance during fieldwork. G Bologne and HJ Bernhardt supervised XRF and microprobe analyses respectively. Comments by Kerry Stanaway have been greatly appreciated.

References

Andersen, D.J., Lindsley, D.H., Davidson, P.M., 1993. QUIlF: a PASCAL program to assess equilibria among Fe-Mg-Ti oxides, pyroxenes, olivine, and quartz. Computers & Geosciences 19, 1333-1350.

Barnes, S.J., 1986. The distribution of chromium among orthopyroxene, spinel and silicate liquid at atmospheric pressure. Geochimica et Cosmochimica Acta 50, 1889-1909.

Bateman, A.M., 1951. The formation of late magmatic oxide ores. Economic Geology 46, 404-426.

Bergeron, M.B., 1986. Minéralogie et géochimie de la suite anorthositique de la région du Lac Allard, Québec: Evolution des membres mafiques et origine des gîtes massifs d'ilménite, PhD Thesis, University of Montreal, 480 pp.

Bourret, W., 1949. Aeromagnetic survey of the Allard Lake district, Quebec. Economic Geology 44, 732-740.

Campbell, I.H., Murck, B.W., 1993. Petrology of the G and H chromitite zones in the Mountain View area of the Stillwater Complex, Montana. Journal of Petrology 34, 291-316.

Carmichael, C.M., 1959. Remanent magnetism of the Allard Lake ilmenites. Nature 183, 1239-1241.

Charlier, B., Duchesne, J.-C., Vander Auwera, J., 2006. Magma chamber processes in the Tellnes ilmenite deposit (Rogaland Anorthosite Province, SW Norway) and the formation of Fe-Ti ores in massif-type anorthosites. Chemical Geology 234, 264-290.

Charlier, B., Skår, Ø., Korneliussen, A., Duchesne, J.-C., Vander Auwera, J., 2007. Ilmenite composition in the Tellnes Fe-Ti deposit, SW Norway: fractional crystallization, postcumulus evolution and ilmenite-zircon relation. Contributions to Mineralogy and Petrology 154, 119-134.

Charlier, B., Sakoma, E., Sauvé, M., Stanaway, K., Vander Auwera, J., Duchesne, J.-C., 2008. The Grader layered intrusion (Havre-Saint-Pierre Anorthosite, Quebec) and genesis of nelsonite and other Fe-Ti-P ores. Lithos 101, 359-378.

Charlier, B., Namur, O., Duchesne, J.-C., Wiszniewska, J., Parecki, A., Vander Auwera, J., 2009. Cumulate origin and polybaric crystallization of Fe-Ti oxide ores in the Suwalki anorthosite, Northeastern Poland. Economic Geology 104, 205-221.

Charlier, B., Storme, J.-Y., Maquil, R., Vander Auwera, J., Longhi, J., Duchesne, J.-C., submitted. Continuous polybaric fractional crystallization of high-alumina basalt parental magmas in the Egersund-Ogna massif-type anorthosite (Rogaland, SW Norway): constraints from plagioclase and high-alumina orthopyroxene megacrysts.

Corrigan, D., van Breemen, O., 1997. U-Pb age constraints for the lithotectonic evolution of the Grenville Province along the Mauricie transect, Quebec. Canadian Journal of Earth Sciences 34, 299-316.

Corriveau, L., Perreault, S., Davidson, A., 2007. Prospective metallogenic settings of the Grenville Province. In: Goodfellow, W.D. (Ed.), Mineral deposits of Canada: A synthesis of major deposit-types, district metallogeny, the evolution of geological provinces, and exploration methods. Geological Survey of Canada, Mineral Deposits Division, Special Publication, pp. 819-847.

Davidson, A., 1995. A review of the Grenville orogen in its North American type area. Journal of Australian Geology and Geophysics 16, 3-24.

Davidson, A., 2008. Late Paleoproterozoic to mid-Neoproterozoic history of northern Laurentia: An overview of central Rodinia. Precambrian Research 160, 5-22.

De Waal, S.A., Xu, Z., Li, C., Mouri, H., 2004. Emplacement of viscous mushes in the Jinchuan ultramafic intrusion, western China. Canadian Mineralogist 42, 371-392.

Duchesne, J.C., 1999. Fe-Ti deposits in Rogaland anorthosites (South Norway): geochemical characteristics and problems of interpretation. Mineralium Deposita 34, 182-198.

Duchesne, J.C., Bologne, G., 2009. XRF major and trace element determination in Fe-Ti oxide minerals. Geologica Belgica 12, 205-212.

Dymek, R.F., 1984. Sapphirine of possible igneous origin from the St-Urbain anorthosite massif, Quebec. EOS 65, 295.

Dymek, R.F., 2001. Observations on the Allard Lake anorthosite, Grenville Provine, Quebec, and implications for petrogenesis of the CRUML belt of massif anorthosites. Geological Society of America Abstracts with Programs 33, 57.

Dymek, R.F., Owens, B.E., 2001. Petrogenesis of apatite-rich rocks (nelsonites and oxide-apatite gabbronorites) associated with massif anorthosites. Economic Geology 96, 797-815.

Eales, H.V., Reynolds, I.M., 1986. Cryptic variations within chromites of the Upper Critical Zone, Northwestern Bushveld Complex. Economic Geology 81, 1056-1066.

Emslie, R.F., 1975. Pyroxene megacrysts from anorthositic rocks: a new clue to the sources and evolution of the parent magmas. Canadian Mineralogist 13, 138-145.

Emslie, R.F., 1985. Proterozoic anorthosite massifs. In: Tobi, A.C., Touret, J.L.R. (Eds), The Deep Proterozoic Crust in the North Atlantic Provinces. Dordrecht, Reidel, pp. 39-60.

Emslie, R.F., Hunt, P.A., 1990. Ages and petrogenetic significance of igneous mangerite charnockite suites associated with massif anorthosites, Grenville Province. Journal of Geology 98, 213-231.

Force, E.R., 1991. Geology of Titanium-Mineral Deposits, US Geological Survey Special Paper, 112 pp.

Hammond, P., 1952. Allard Lake ilmenite deposits. Economic Geology 47, 634-649.

Hargraves, R.B., 1959. Magnetic anisotropy and remanent magnetization in hemo-ilmenite from ore deposits of Allard Lake, Quebec. Journal of Geophysical Research 64, 1565-1573.

Hargraves, R.B., 1962. Petrology of the Allard Lake anorthosite suite, Quebec. In: Engel, A. E.J., James, H.L., Leonard, B.F. (Eds), Petrologic studies: a volume to honor A.F. Buddington. Geological Society of America, Denver, pp. 163-189.

Hébert, C., Cadieux, A.-M., van Breemen, O., 2005. Temporal evolution and nature of Ti-Fe-P mineralization in the anorthosite-mangerite-charnockite-granite (AMCG) suites of the south-central Grenville Province, Saguenay - Lac St. Jean area, Quebec, Canada. Canadian Journal of Earth Sciences 42, 1865-1880.

Higgins, M.D., 1998. Origin of anorthosite by textural coarsening: Quantitative measurements of a natural sequence of textural development. Journal of Petrology 39, 1307-1323.

Higgins, M.D., van Breemen, O., 1996. Three generations of Anorthosite-Mangerite-Charnockite-Granite magmatism, contact metamorphism and tectonism in the Saguenay-Lac-St-Jean region, Grenville Province, Canada. Precambrian Research 79, 347-362.

Hocq, M., 1982. Région du Lac Allard. Ministère de l’Energie et Ressources, Québec DPV-894, 99 pp.

Irvine, T.N., 1975. Crystallization sequences in the Muskox intrusion and other layered intrusions - II. Origin of chromitite layers and similar deposits of other magmatic ores. Geochimica et Cosmochimica Acta 39, 991-1020.

Irvine, T.N., 1977. Origin of chromitite layers in the Muskox intrusion and other stratiform intrusions: a new interpretation. Geology 5, 273-277.

Kinnaird, J.A., Kruger, F.J., Nex, P.A.M., Cawthorn, R.G., 2002. Chromitite formation - a key to understanding processes of platinum enrichment. Transactions of the Institution of Mining and Metallurgy 111, 23-35.

Klemme, S., Gunther, D., Hametner, K., Prowatke, S., Zack, T., 2006. The partitioning of trace elements between ilmenite, ulvospinel, armalcolite and silicate melts with implications for the early differentiation of the moon. Chemical Geology 234, 251-263.

Kolker, A., 1982. Mineralogy and geochemistry of Fe-Ti oxide and apatite (nelsonite) deposits and evaluation of the liquid immiscibility hypothesis. Economic Geology 77, 1146-1148.

Li, C., Naldrett, A.J., 1999. Geology and petrology of the Voisey's Bay intrusion: reaction of olivine with sulfide and silicate liquids. Lithos 47, 1-31.

Li, C.S., Xu, Z.H., de Waal, S.A., Ripley, E.M., Maier, W.D., 2004. Compositional variations of olivine from the Jinchuan Ni-Cu sulfide deposit, western China: implications for ore genesis. Mineralium Deposita 39, 159-172.

Lindsley, D.H., 2003. Do Fe-Ti oxide magmas exist? Geology: Yes; Experiments: No! Norges Geologiske Undersøkelse Special Publication 9, 34-35.

Lister, G.F., 1966. The composition and origin of selected iron-titanium deposits. Economic Geology 61, 275-310.

Longhi, J., Vander Auwera, J., Fram, M., Monthieth, J.N., 1993. Pressure effects, kinetics and rheology of anorthositic and related magmas. American Mineralogist 78, 1016-1030.

Maier, W.D., Li, C., De Waal, S.A., 2001. Why are there no major Ni-Cu sulfide deposits in large layered mafic-ultramafic intrusions? Canadian Mineralogist 39, 547-556.

McEnroe, S.A., Robinson, P., Langenhorst, F., Frandsen, C., Terry, M.P., Boffa Ballaran, T., 2007. Magnetization of exsolution intergrowths of hematite and ilmenite: Mineral chemistry, phase relations, and magnetic properties of hemo-ilmenite ores with micron- to nanometer-scale lamellae from Allard Lake, Quebec. Journal of Geophysical Research 112, B10103.

Mondal, S.K., Mathez, E.A., 2007. Origin of the UG2 chromitite layer, Bushveld Complex. Journal of Petrology 48, 495-510.

Morisset, C.-E., Scoates, J.S., 2008. Origin of zircon rims around ilmenite in mafic plutonic rocks of Proterozoic anorthosite suites. Canadian Mineralogist 46, 289-304.

Morisset, C.-E., Scoates, J.S., Weis, D., Friedman, R.M., 2009. U-Pb and $^{40}Ar/^{39}Ar$ geochronology of the Saint-Urbain and Lac Allard (Havre-Saint-Pierre) anorthosites and their associated Fe-Ti oxide ores, Québec: Evidence for emplacement and slow cooling during the collisional Ottawan orogeny in the Grenville Province. Precambrian Research 174, 95-116.

Morisset, C.-E., Scoates, J.S., Weis, D., Sauvé, M., Stanaway, K., submitted. Rutile-bearing ilmenite deposits associated with Proterozoic massifs of the Grenville Province (Québec). Canadian Mineralogist.

Murck, B.W., Campbell, I.H., 1986. The effects of temperature, oxygen fugacity and melt composition on the behaviour of chromium in basic and ultrabasic melts. Geochimica et Cosmochimica Acta 50, 1871-1887.

Owen, J.V., Greenough, J.D., 1991. An empirical sapphirine-spinel Mg-Fe exchange thermometer and its application to high grade xenoliths in the Popes Harbour dyke, Nova Scotia, Canada. Lithos 26, 317-332.

Owens, B.E., Dymek, R.F., 2001. Petrogenesis of the Labrieville alkalic anorthosite massif, Grenville Province, Quebec. Journal of Petrology 42, 1519-1546.

Owens, B.E., Dymek, R.F., 2005. Rediscovery of the Mattawa anorthosite massif, Grenville Province, Quebec. Canadian Journal of Earth Sciences 42, 1699-1718.

Owens, B.E., Dymek, R.F., Tucker, R.D., Brannon, J.C., Podosek, F.A., 1994. Age and radiogenic isotopic composition of a late- to posttectonic anorthosite in the Grenville Province - the Labrieville massif, Quebec. Lithos 31, 189-206.

Pang, K.-N., Li, C., Zhou, M.-F., Ripley, E., 2008. Abundant Fe-Ti oxide inclusions in olivine from the Panzhihua and Hongge layered intrusions, SW China: evidence for early saturation of Fe-Ti oxides in ferrobasaltic magma. Contributions to Mineralogy and Petrology 156, 307-321.

Pang, K.-N., Li, C., Zhou, M.-F., Ripley, E.M., 2009. Mineral compositional constraints on petrogenesis and oxide ore genesis of the late Permian Panzhihua layered gabbroic intrusion, SW China. Lithos 110, 199-214.

Philpotts, A.R., 1967. Origin of certain iron-titanium oxide and apatite rocks. Economic Geology 62, 303-315.

Rivers, T., 1997. Lithotectonic elements of the Grenville Province: review and tectonic implications. Precambrian Research 86, 117-154.

Rivers, T., 2008. Assembly and preservation of lower, mid, and upper orogenic crust in the Grenville Province - Implications for the evolution of large hot long-duration orogens. Precambrian Research 167, 237-259.

Rivers, T., Corrigan, D., 2000. Convergent margin on southeastern Laurentia during the Mesoproterozoic: tectonic implications. Canadian Journal of Earth Sciences 37, 359-383.

Rivers, T., Martignole, J., Gower, C.F., Davidson, A., 1989. New tectonic divisions of the Grenville Province, southeastern Canadian Shield. Tectonics 8, 63-84.

Rivers, T., Ketchum, J., Indares, A., Hynes, A., 2002. The High Pressure belt in the Grenville Province: architecture, timing, and exhumation. Canadian Journal of Earth Sciences 39, 867-893.

Roeder, P.L., Reynolds, I.M., 1991. Crystallization of chromite and chromium solubility in basaltic melts. Journal of Petrology 32, 909-934.

Romer, R.L., 1996. Contiguous Laurentia and Baltica before the Grenvillian-Sveconorwegian orogeny? Terra Nova 8, 173-181.

Sharma, K.N.M., Franconi, A., 1975. Magpie, Saint-Jean, Romaine Rivers area (Grenville 1970). Québec Ministère des Ressources Naturelles Geological Report 163, 73 pp.

Toplis, M.J., Carroll, M.R., 1995. An experimental study of the influence of oxygen fugacity on Fe-Ti oxide stability, phase relations, and mineral-melt equilibria in ferro-basaltic systems. Journal of Petrology 36, 1137-1170.

van Breemen, O., Higgins, M.D., 1993. U-Pb zircon age of the southwest lobe of the Havre-Saint-Pierre Anorthosite Complex, Grenville Province, Canada. Canadian Journal of Earth Sciences 30, 1453-1457.

Warren, C.H., 1912. The ilmenite rock near St. Urbain: a new occurrence of rutile and sapphirine. American Journal of Science 33, 263-277.

Wilson, J.R., Robins, B., Nielsen, F.M., Duchesne, J.C., Vander Auwera, J., 1996. The Bjerkreim-Sokndal layered intrusion, Southwest Norway. In: Cawthorn, R.G. (Ed), Layered Intrusions. Elsevier, Amsterdam, pp. 231-255.

Wodicka, N., David, J., Parent, M., Gobeil, A., Verpaelst, P., 2003. Géochronologie U-Pb et Pb-Pb de la région de Sept-Îles - Natashquan, Province de Grenville, Moyenne-Côte-Nord. In: Brisebois, D. and Clark, T. (Editors) Géologie et Ressources minérales de la partie est de la Province de Grenville. Ministère des Ressources naturelles de la Faune et des Parcs, Québec, DV 2002-03, pp. 59-117.

Zhou, M.-F., Robinson, P.T., Lesher, C.M., Keays, R.R., Zhang, C.-J., Malpas, J., 2005. Geochemistry, petrogenesis and metallogenesis of the Panzhihua gabbroic layered intrusion and associated Fe-Ti-V oxide deposits, Sichuan Province, SW China. Journal of Petrology 46, 2253-2280.

Figure captions

Fig. 1. Simplified geological map of the Grenville Province showing the geological subdivisions into parautochtonous and allochtonous belts (after Rivers et al., 1989; Davidson, 1995; Wodicka et al., 2003; Corriveau et al., 2007) and the major Proterozoic pre-Grenvillian and Grenvillian anorthosite-mangerite-charnockite-granite suites.

Fig. 2. Geological map of the Havre-Saint-Pierre anorthosite complex (after Wodicka et al., 2003), with location of the Allard Lake deposit and the Grader layered intrusion. Numbers 1 and 2 are locations of samples for geochronology, in the Rivière au Tonnerre anorthosite and in the Magpie River monzonitic envelope respectively.

Fig. 3. Detailed views of the Allard Lake deposit. (a) Contour map of the deposit with location of samples TL (stars) and of drill-cores (black circles are drill-cores sampled for plagioclase and ilmenite separation and grey squares are mining drill-cores used for whole-rock analyses; Coordinates are UTM - Nad 83, Zone 20N); (b) Aerial picture of the deposit showing the open-pit in 2008; (c-d) 3D modelling of the morphology of the deposit using 172643 mining ore samples (GOCAD software). Colour scale is for the depth.

Fig. 4. Histograms of the ilmenite proportion in the Allard Lake ilmenite deposit (n=172643) compared to that in the Tellnes deposit (n=94; data from Charlier et al., 2006).

Fig. 5. Photomicrographs of the main rock types and ilmenite textures in the Allard Lake deposit. (a) Typical anorthosite with statically recrystallized plagioclase displaying 120° triple junction (cross-polarized transmitted light, N10-152); (b) Moderately recrystallized

anorthosite showing abundant orthoclase needles at the margin of plagioclase laths and interstitial quartz (cross-polarized transmitted light, T875-297); (c) Norite (transmitted light , T875-66); (d) Ilmenitite with polygonized ilmenite grains (reflected light, T873-178); (e) Small aluminous spinel granule in hemo-ilmenite; note the decreasing amount of hematite lamellae close to spinel (reflected and transmitted lights, T873-224); (f) Hemo-ilmenite grain in contact with plagioclase, with a zircon corona (backscattered electron images, T873-219). Abbreviations: Pl = plagioclase, Ilm = ilmenite, Hem = hematite, Opx = orthopyroxene, Sp = aluminous spinel, Zrn = zircon.

Fig. 6. Photomicrographs of the main textures of orthopyroxene and sapphirine in the Allard Lake ilmenite deposit. (a) Orthopyroxene with Schiller-type exsolution and included grains of hemo-ilmenite (reflected and transmitted light, T873-133); (b) Symplectitic intergrowth of high-alumina orthopyroxene and vermicular aluminous spinel (reflected and transmitted light, T873-291); (c) Small sapphirine grain at the contact between ilmenite and orthopyroxene (transmitted light, T873-268); (d) Sapphirine grain at the junction between orthopyroxene and aluminous spinel (reflected and transmitted lights, T873-68). Same abbreviations as in Fig. 5; Spr = sapphirine.

Fig. 7. Stratigraphic variation of ilmenite composition and ilmenite proportion in holes T873, T875 and N10 (see location on Fig. 3).

Fig. 8. Histograms of the composition of plagioclase for the contents of anorthite, orthoclase, Sr and Ba. Data for different rock types are stacked.

Fig. 9. Compositional profiles for $X_{hercynite}$ and Cr_2O_3 across aluminous spinel in sample T873-296. The distance scale is from an arbitrary starting point and only relative distances have any significance.

Fig. 10. Enstatite (100[Mg/(Mg+Fe+Ca)]) and Wollastonite (100[Ca/(Mg+Fe+Ca)]) as a function of Al_2O_3 in orthopyroxene.

Fig. 11. Binary major elements variation diagrams of whole-rocks from the Allard Lake ilmenite deposit. The compositional ranges of main minerals are represented by a elliptic area or indicated by an arrow (plag = plagioclase, ilm = ilmenite, opx = orthopyroxene). Note that both high- and low-alumina orthopyroxenes are plotted.

Fig. 12. Calculated Cr concentration in ilmenite (ppm) in selected holes of the Allard Lake ilmenite deposit. The calculation is based on whole-rock TiO_2 and Cr contents and an average TiO_2 content in ilmenite of 37.71 wt.%.

Fig. 13. Cr (ppm) as a function of V (ppm) in ilmenite from the Allard Lake ilmenite deposit with Rayleigh fractional crystallization models for X_{ilm}=1 (fractionation of ilmenite alone) and for X_{ilm}=0.21 and 0.16 (fractionation of a cotectic ilmenite-plagioclase cumulate) using a starting composition of ilmenite with Cr=2415 ppm and V=2380 ppm. Note the values for the fraction of residual liquid on crystallization paths. Partition coefficients from Charlier et al. (2008). Black symbols represent ilmenite composition from mineral separates and grey points are calculated ilmenite compositions from the whole-rock mining database.

Fig. 14. Histograms of the Cr content in ilmenite (ppm) in the Allard Lake ilmenite deposit compared to that in the Grader layered intrusion (data from Charlier et al., 2008).

Figure1

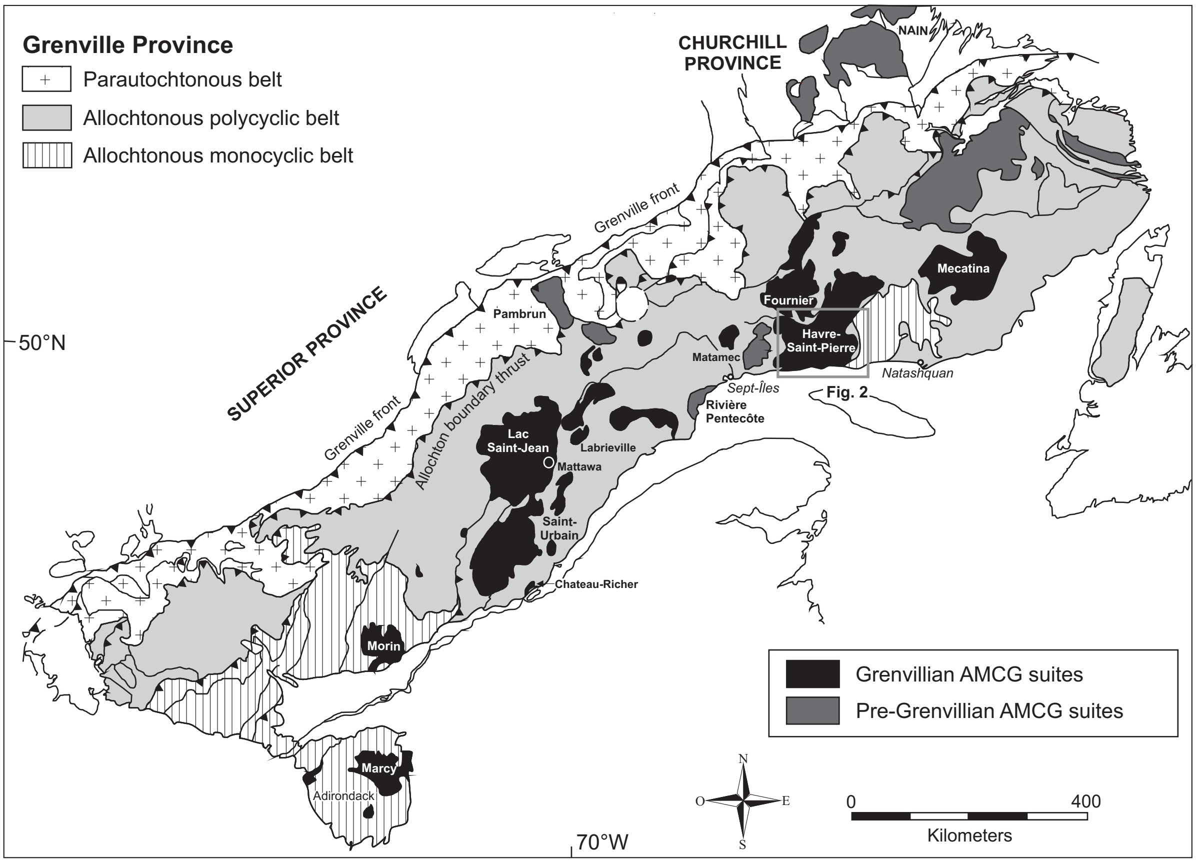

Grenville Province
Paraautochtonous belt
Allochtonous polycyclic belt
Allochtonous monocyclic belt
CHURCHILL PROVINCE
NAIN
SUPERIOR PROVINCE
Grenville front
Grenville front
Allochton boundary thrust
Pambrun
Mecatina
Fournier
Havre-Saint-Pierre
Matamec
Sept-Îles
Natashquan
Fig. 2
Rivière Pentecôte
Lac Saint-Jean
Labrieville
Mattawa
Saint-Urbain
Chateau-Richer
Morin
Marcy
Adirondack
50°N
70°W
Grenvillian AMCG suites
Pre-Grenvillian AMCG suites
N
O
E
S
0
400
Kilometers

Figure2

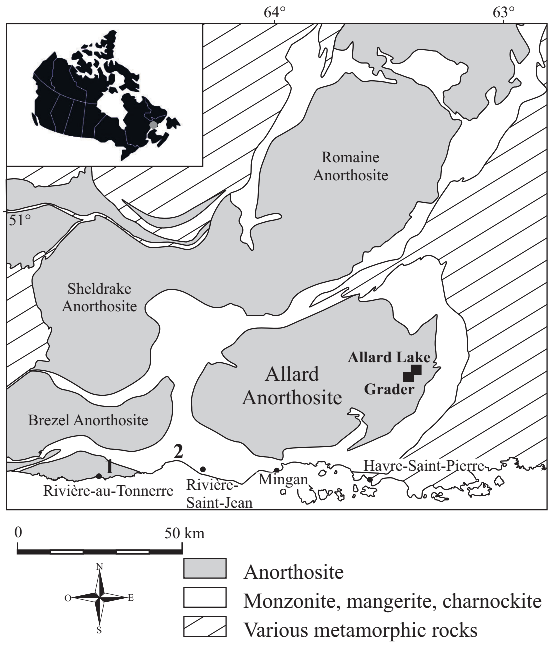
64°
63°
51°
Romaine Anorthosite
Sheldrake Anorthosite
Allard Anorthosite
Allard Lake
Grader
Brezel Anorthosite
1
2
Rivière-au-Tonnerre
Rivière-Saint-Jean
Mingan
Havre-Saint-Pierre
0
50 km
N
O
E
S
Anorthosite
Monzonite, mangerite, charnockite
Various metamorphic rocks

Figure3

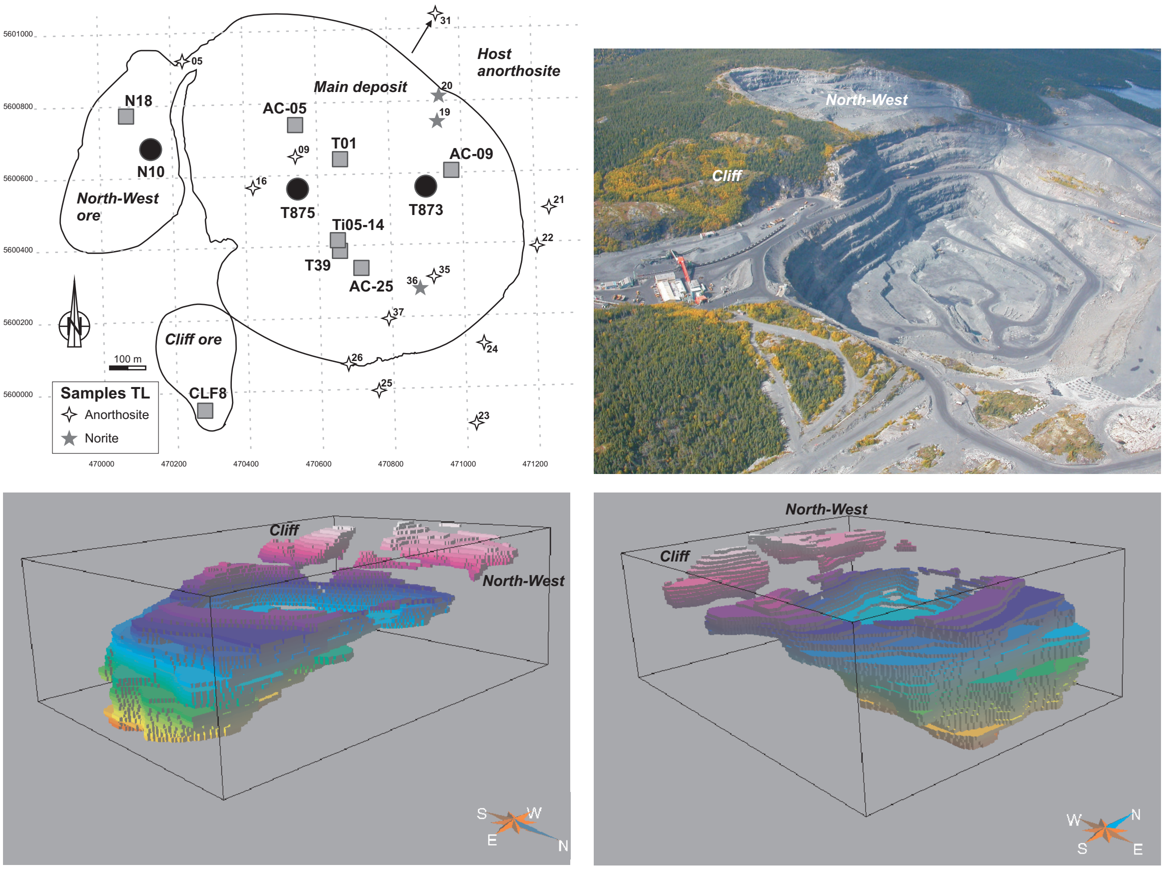

5601000
5600800
5600600
5600400
5600200
5600000
470000
470200
470400
470600
470800
471000
471200
Host anorthosite
Main deposit
North-West ore
Cliff ore
N18
N10
AC-05
T01
AC-09
T875
T873
Ti05-14
T39
AC-25
CLF8
05
09
16
19
20
21
22
23
24
25
26
31
35
36
37
100 m
Samples TL
Anorthosite
Norite
North-West
Cliff
Cliff
North-West
S
W
E
N
North-West
Cliff
W
N
S
E

Figure4

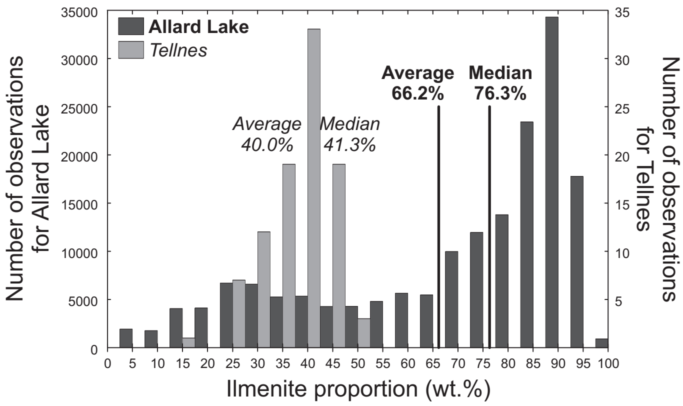

Allard Lake
Tellnes
Average
40.0%
Median
41.3%
Average
66.2%
Median
76.3%
Number of observations for Allard Lake
Number of observations for Tellnes
Ilmenite proportion (wt.%)
0
5000
10000
15000
20000
25000
30000
35000
0 5 10 15 20 25 30 35 40 45 50 55 60 65 70 75 80 85 90 95 100

Figure5

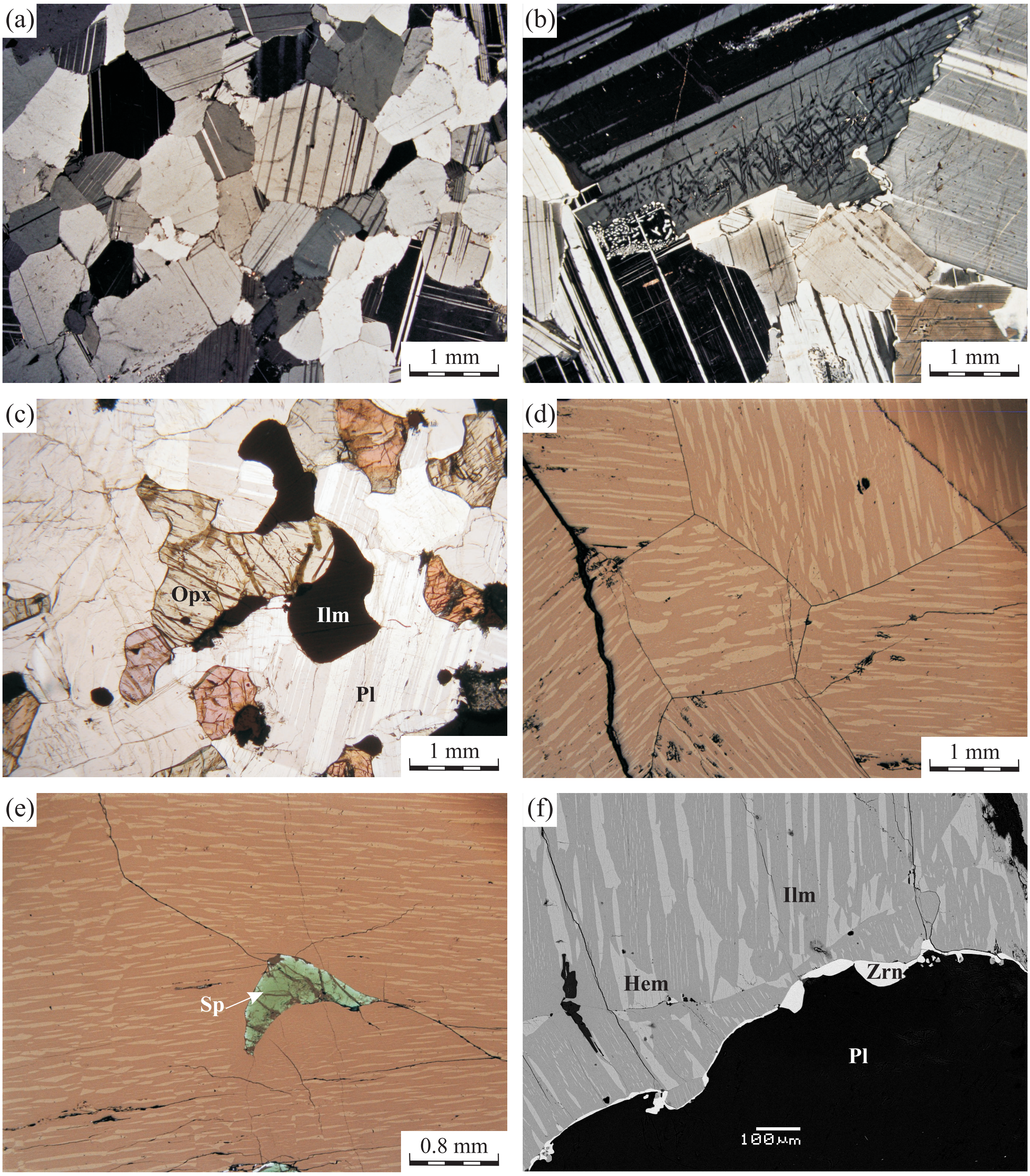

Figure6

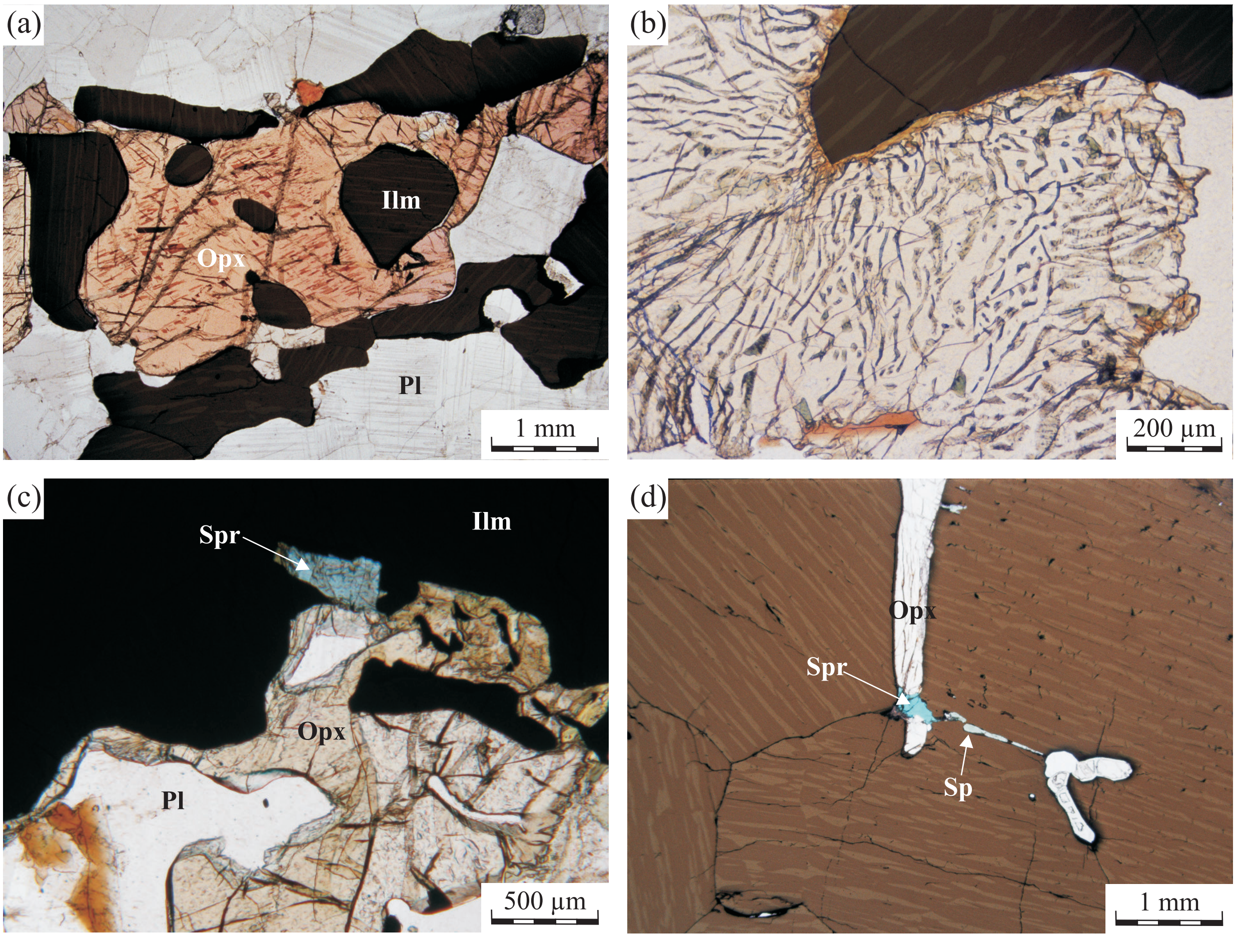

Figure7

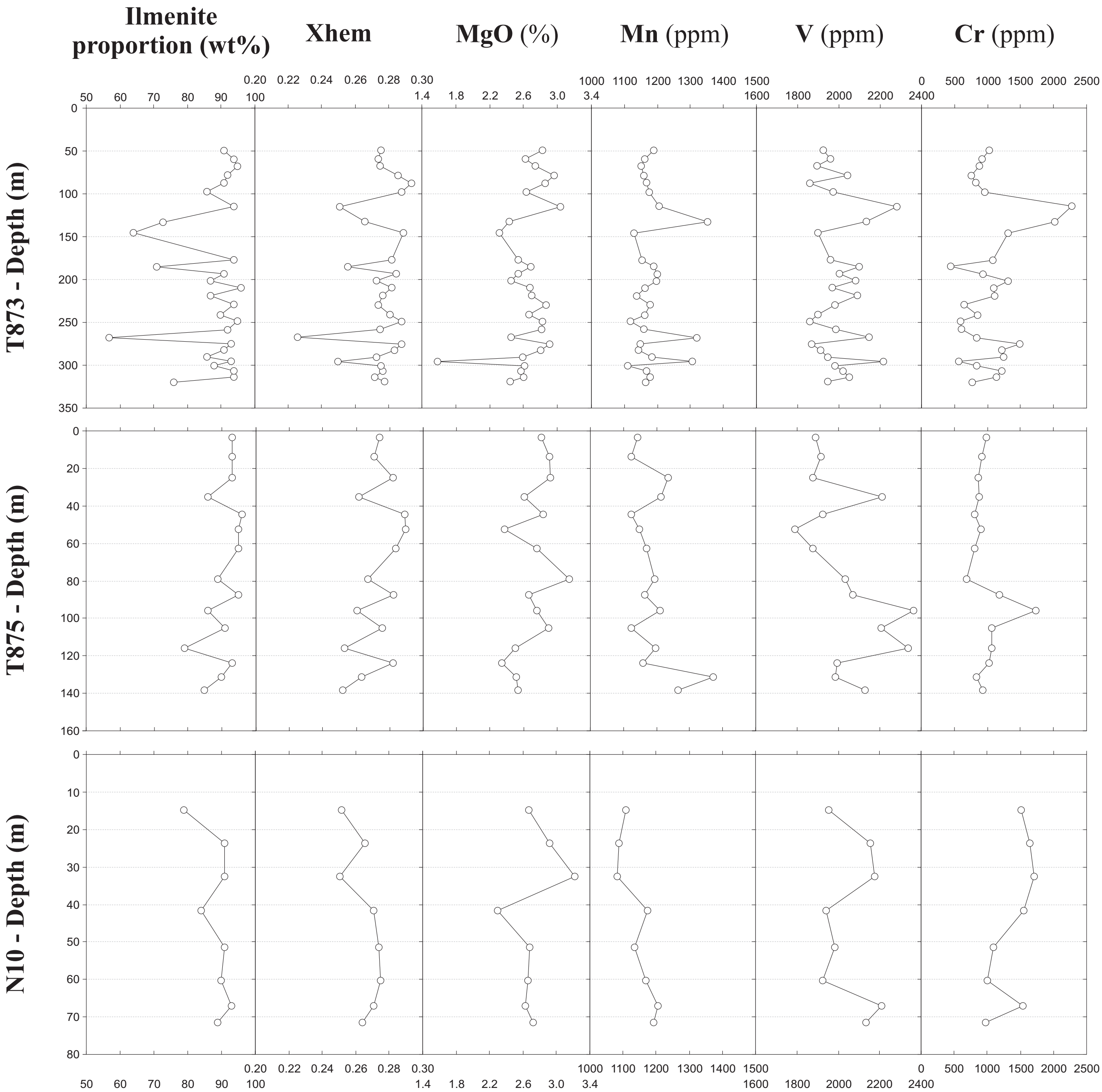
Ilmenite proportion (wt%)
Xhem
MgO (%)
Mn (ppm)
V (ppm)
Cr (ppm)
T873 - Depth (m)
T875 - Depth (m)
N10 - Depth (m)

Figure8

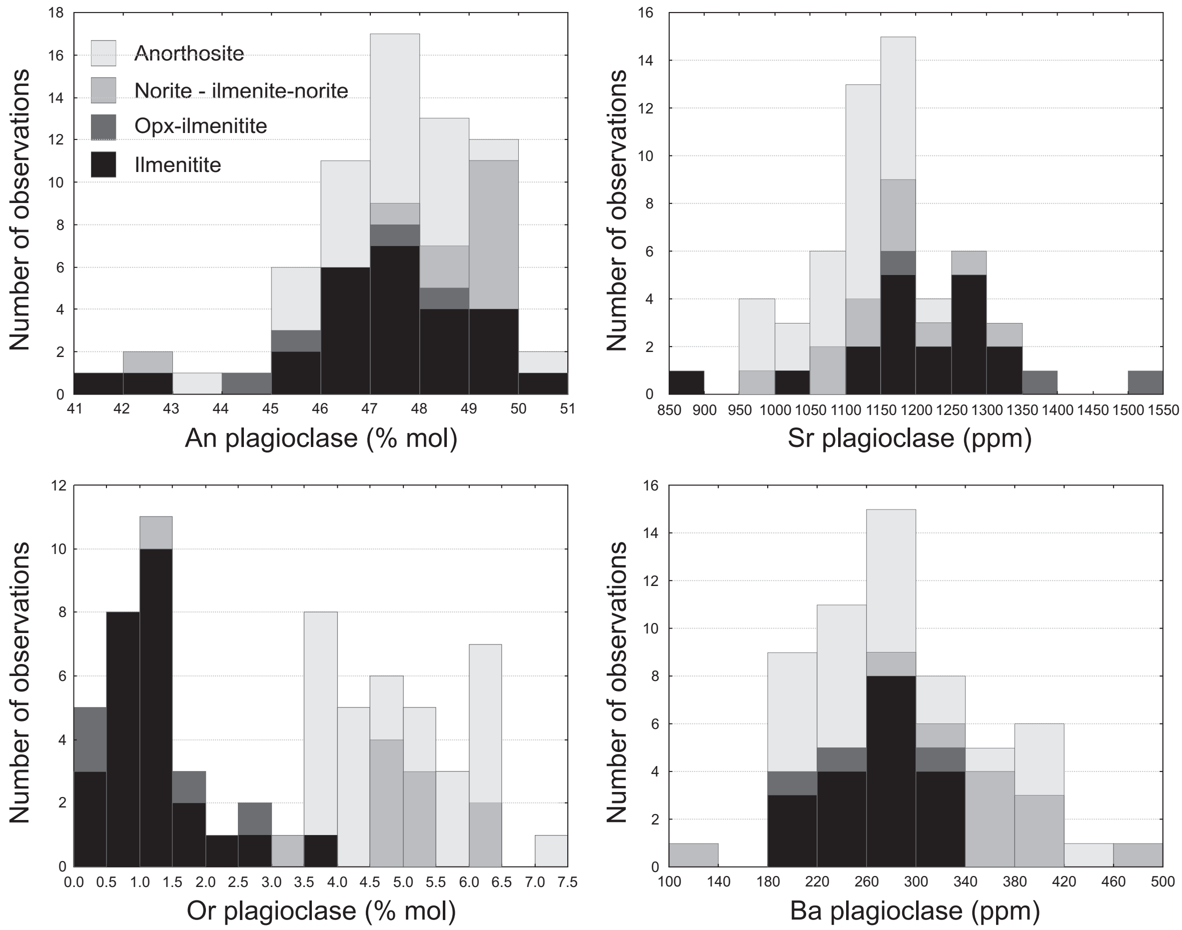
Anorthosite
Norite - ilmenite-norite
Opx-ilmenitite
Ilmenitite
Number of observations
An plagioclase (% mol)
Sr plagioclase (ppm)
Or plagioclase (% mol)
Ba plagioclase (ppm)

Figure9

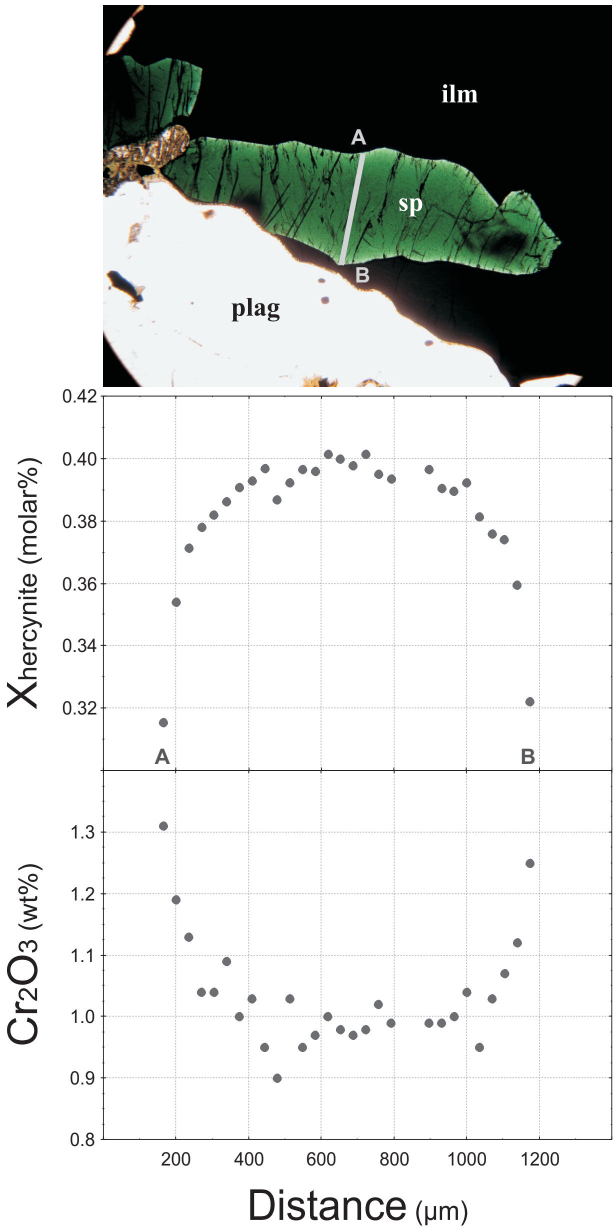
ilm
A
sp
B
plag
0.42
0.40
0.38
0.36
0.34
0.32
Xhercynite (molar%)
A
B
1.3
1.2
1.1
1.0
0.9
0.8
Cr2O3 (wt%)
200
400
600
800
1000
1200
Distance (µm)

Figure10

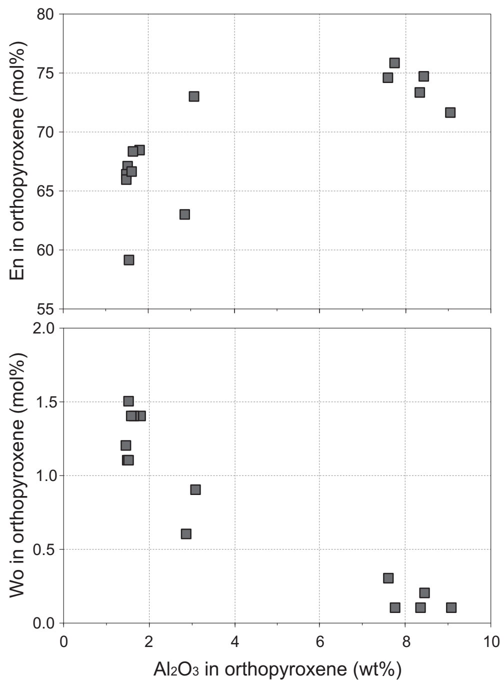

80
75
70
65
60
55
En in orthopyroxene (mol%)
2.0
1.5
1.0
0.5
0.0
Wo in orthopyroxene (mol%)
0
2
4
6
8
10
Al2O3 in orthopyroxene (wt%)

Figure11

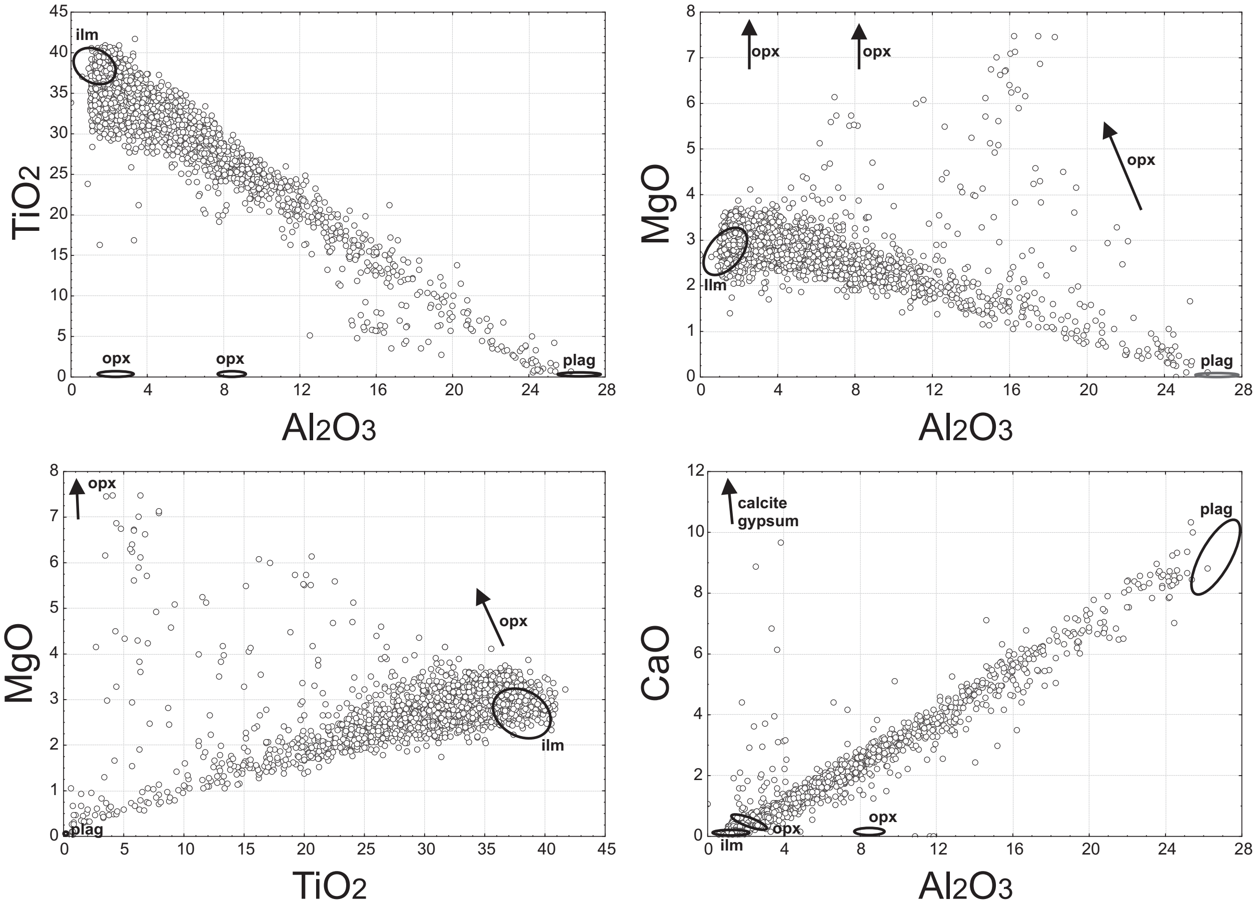

ilm
opx
opx
plag
TiO2
Al2O3
opx
opx
opx
MgO
Ilm
plag
Al2O3
opx
opx
MgO
ilm
plag
TiO2
calcite
gypsum
plag
CaO
ilm
opx
opx
Al2O3

Figure12

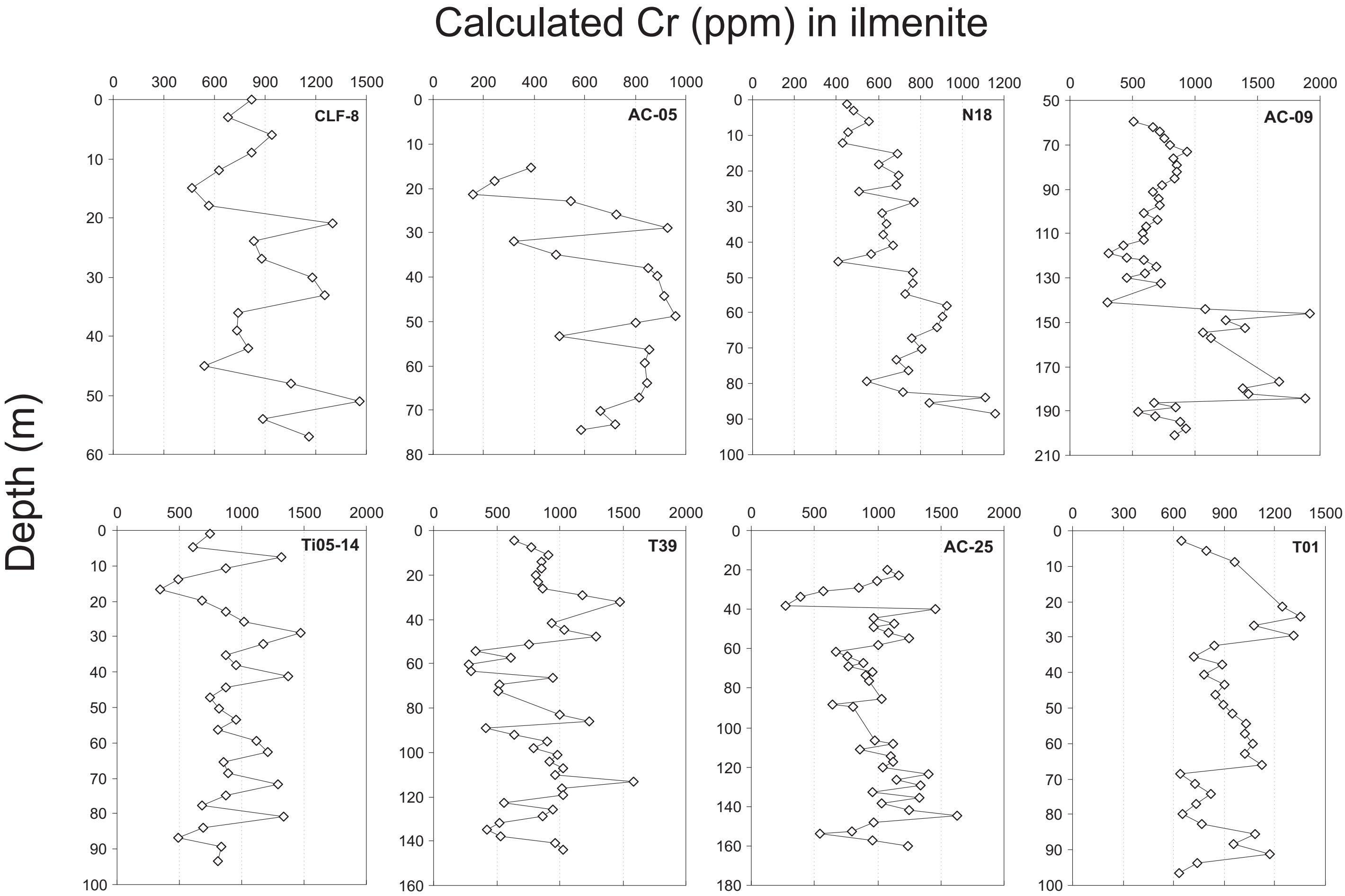

Calculated Cr (ppm) in ilmenite
Depth (m)
CLF-8
AC-05
N18
AC-09
Ti05-14
T39
AC-25
T01

Figure13

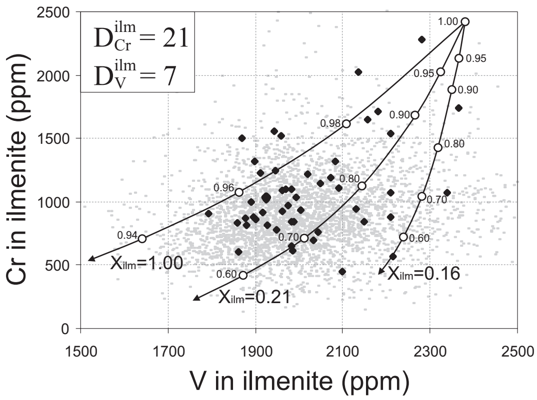

$D_{Cr}^{ilm} = 21$
$D_{V}^{ilm} = 7$
Cr in ilmenite (ppm)
V in ilmenite (ppm)
2500
2000
1500
1000
500
0
1500
1700
1900
2100
2300
2500
1.00
0.95
0.95
0.90
0.90
0.98
0.80
0.80
0.96
0.70
0.70
0.94
0.60
0.70
0.60
X_{ilm}=1.00
X_{ilm}=0.21
X_{ilm}=0.16

Figure14

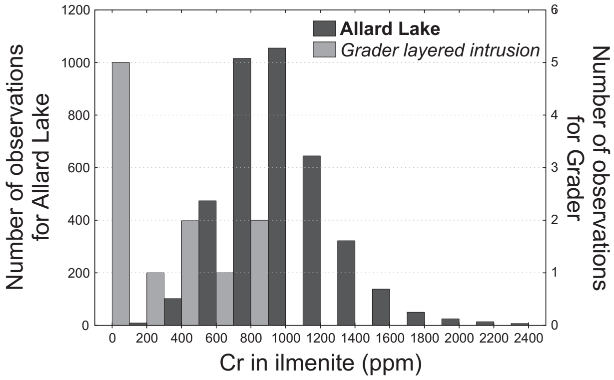
Allard Lake
Grader layered intrusion
Number of observations for Allard Lake
Number of observations for Grader
Cr in ilmenite (ppm)
0
200
400
600
800
1000
1200
1400
1600
1800
2000
2200
2400
1
2
3
4
5
6

Table1
Click here to download Table: Table1.xls

Table 1
XRF analyses of separated ilmenite from the Allard lake ilmenite deposit

Sample	Ilm prop	TiO_2	Al_2O_3	Fe_2O_{3tot}	Fe_2O_3	FeO	MgO	Total	Xgeik	Xpyr	Xhem	Xilm	V	Cr	Zn	Mn	Zr	Nb
T873-50	91	37.81	1.26	61.58	29.57	28.80	2.83	100.27	0.105	0.003	0.276	0.616	1924	1036	122	1189	274	31
T873-60	94	37.73	1.34	61.61	29.28	29.09	2.63	100.07	0.098	0.003	0.274	0.625	1963	924	139	1162	776	21
T873-68	95	37.48	0.72	60.77	28.91	28.67	2.74	98.52	0.103	0.003	0.275	0.618	1895	883	90	1152	243	26
T873-79	92	37.28	1.29	61.84	30.64	28.08	2.97	100.26	0.110	0.003	0.286	0.601	2043	763	132	1159	195	33
T873-88	91	36.64	1.68	62.36	31.58	27.70	2.86	100.46	0.105	0.003	0.294	0.597	1859	829	194	1168	659	32
T873-98	86	36.77	1.45	61.99	30.64	28.21	2.64	99.71	0.098	0.003	0.288	0.611	1975	970	134	1177	183	33
T873-115	94	38.90	1.21	59.41	26.74	29.40	3.04	99.29	0.113	0.003	0.251	0.632	2282	2277	103	1206	281	27
T873-133	73	38.41	0.60	61.52	28.16	30.01	2.44	99.62	0.091	0.004	0.266	0.639	2136	2025	85	1352	24	29
T873-146	64	36.92	0.74	62.61	30.48	28.91	2.32	99.37	0.087	0.003	0.289	0.621	1898	1320	60	1131	188	36
T873-178	94	37.20	1.34	61.93	29.95	28.77	2.54	99.80	0.095	0.003	0.282	0.621	1963	1093	148	1156	371	29
T873-186	71	38.93	0.83	60.62	27.21	30.06	2.69	99.72	0.100	0.003	0.256	0.641	2098	450	65	1190	66	29
T873-194	91	36.85	1.54	61.90	30.29	28.45	2.54	99.67	0.095	0.003	0.285	0.617	2004	937	130	1201	255	32
T873-202	87	38.08	0.45	61.92	28.91	29.71	2.46	99.61	0.092	0.003	0.273	0.631	2084	1321	28	1198	296	33
T873-210	96	37.28	1.38	61.85	30.07	28.59	2.68	100.00	0.099	0.003	0.282	0.616	1970	1099	132	1164	334	28
T873-219	87	37.32	1.59	61.27	29.49	28.59	2.70	99.69	0.100	0.003	0.277	0.620	2090	1110	134	1139	422	36
T873-230	94	37.40	1.66	60.74	29.22	28.36	2.87	99.51	0.107	0.003	0.274	0.616	1984	650	167	1178	214	28
T873-242	90	37.23	1.61	61.86	30.11	28.57	2.67	100.19	0.099	0.003	0.281	0.617	1901	858	155	1164	642	22
T873-249	95	36.74	1.62	61.71	30.76	27.85	2.83	99.80	0.105	0.003	0.288	0.604	1862	601	182	1120	771	33
T873-259	92	37.77	1.31	61.37	29.38	28.78	2.82	100.06	0.104	0.003	0.275	0.618	1986	615	132	1161	56	33
T873-268	57	40.29	0.92	59.17	23.97	31.67	2.46	99.31	0.092	0.004	0.226	0.678	2149	845	46	1321	23	34
T873-276	93	36.64	1.94	61.56	30.88	27.61	2.91	99.98	0.108	0.003	0.288	0.601	1870	1500	218	1150	636	30
T873-283	91	36.81	1.57	61.22	30.17	27.94	2.81	99.30	0.105	0.003	0.284	0.608	1912	1226	163	1143	1261	23
T873-291	86	37.17	1.15	60.38	28.55	28.64	2.60	98.11	0.098	0.003	0.273	0.625	1946	1246	106	1184	1016	26
T873-296	93	38.87	0.76	61.74	26.24	31.94	1.59	99.40	0.060	0.004	0.250	0.687	2216	572	94	1306	22	33
T873-301	88	37.13	1.95	61.19	29.43	28.58	2.62	99.71	0.097	0.003	0.276	0.624	1983	847	160	1111	469	31
T873-307	94	37.31	1.42	61.45	29.42	28.82	2.57	99.54	0.096	0.003	0.277	0.624	2020	1218	153	1168	978	24
T873-314	94	37.65	1.37	61.27	28.98	29.05	2.61	99.66	0.097	0.003	0.272	0.627	2050	1144	170	1179	246	27
T873-320	76	38.14	0.49	62.69	29.60	29.78	2.45	100.46	0.091	0.003	0.278	0.628	1948	778	35	1166	273	34
T875-4	93	37.81	1.17	61.25	29.22	28.82	2.82	99.84	0.105	0.003	0.274	0.618	1891	995	96	1143	139	29
T875-14	93	37.98	1.52	61.09	29.09	28.80	2.92	100.31	0.108	0.003	0.271	0.618	1916	918	134	1125	390	29
T875-25	93	37.21	1.74	61.53	30.33	28.08	2.93	100.29	0.108	0.003	0.282	0.606	1877	870	185	1236	457	36
T875-35	86	38.28	1.10	60.66	27.76	29.61	2.61	99.36	0.098	0.003	0.262	0.637	2211	883	111	1215	177	32
T875-45	96	37.16	1.29	62.30	30.96	28.20	2.84	100.45	0.105	0.003	0.289	0.603	1927	811	116	1126	307	29
T875-53	95	36.52	0.90	61.97	30.36	28.45	2.38	98.61	0.090	0.003	0.290	0.617	1793	904	91	1149	288	31
T875-63	95	37.26	1.36	61.89	30.31	28.42	2.77	100.12	0.103	0.003	0.284	0.611	1879	811	129	1170	554	30
T875-79	89	37.93	1.93	60.27	28.77	28.34	3.15	100.12	0.116	0.003	0.267	0.613	2034	693	185	1196	150	24
T875-87	95	37.49	0.96	62.13	30.12	28.81	2.67	100.05	0.099	0.003	0.283	0.615	2072	1192	91	1167	354	35
T875-96	86	38.02	1.59	60.01	27.68	29.09	2.77	99.15	0.103	0.003	0.261	0.632	2365	1743	138	1213	163	26
T875-105	91	37.58	1.65	61.17	29.55	28.45	2.91	100.14	0.108	0.003	0.276	0.614	2210	1076	133	1125	232	32
T875-116	79	38.64	0.43	59.79	26.32	30.12	2.51	98.02	0.095	0.003	0.253	0.649	2339	1072	30	1199	153	25
T875-124	93	37.22	0.91	62.17	29.80	29.13	2.35	99.41	0.088	0.003	0.282	0.627	1994	1032	101	1160	250	38
T875-131	90	38.13	1.22	60.88	27.96	29.63	2.52	99.46	0.094	0.004	0.264	0.639	1987	846	126	1373	436	31
T875-139	85	38.64	1.29	60.04	26.64	30.06	2.54	99.17	0.095	0.003	0.252	0.650	2131	939	104	1266	279	39
N10-15	79	38.83	0.82	59.95	26.59	30.02	2.67	98.93	0.100	0.003	0.252	0.645	1958	1517	70	1110	240	28
N10-24	91	38.08	1.51	60.62	28.51	28.90	2.92	99.92	0.108	0.003	0.266	0.622	2158	1649	147	1088	298	30
N10-33	91	38.80	1.53	59.04	26.80	29.01	3.22	99.36	0.120	0.003	0.251	0.626	2180	1710	123	1084	222	22
N10-42	84	37.76	0.86	61.56	28.55	29.70	2.30	99.17	0.086	0.003	0.271	0.639	1944	1553	69	1176	525	33
N10-52	91	37.75	1.32	61.46	29.23	29.00	2.69	99.99	0.100	0.003	0.274	0.623	1984	1099	120	1137	369	27
N10-60	90	37.58	1.35	61.48	29.36	28.90	2.66	99.85	0.099	0.003	0.275	0.622	1925	1012	113	1171	375	36
N10-67	93	37.91	1.53	61.49	28.99	29.24	2.63	100.30	0.097	0.003	0.271	0.629	2210	1540	148	1208	483	27

Major elements in weight percent, FeO and Fe_2O_3 recalculated from Fe_2O_{3tot} by charge balance; molar fractions of geikielite ($MgTiO_3$), pyrophanite ($MnTiO_3$), hematite (Fe_2O_3) and ilmenite ($FeTiO_3$) (Xgeik, Xpyr, Xhem, Xilm) calculated following QUILF algorithm (Andersen et al., 1993); trace elements in parts per million (ppm)

Table 2

Major and trace element compositions of separated plagioclase from the Allard lake ilmenite deposit and the host Havre-Saint-Pierre anorthosite (XRF analyses)

Sample	Ilm prop	Rock type	SiO_2	TiO_2	Al_2O_3	Fe_2O_3	CaO	Na_2O	K_2O	Total	An	Or	Ba	Sr
T873-16	33	opx-norite	56.27	0.06	26.89	0.31	9.33	5.32	0.92	99.30	49.2	5.5	402	1176
T873-31	44	norite	56.19	0.08	26.77	0.41	9.09	5.21	1.08	99.13	49.1	6.5	409	1161
T873-50	91	ilmenitite	55.41	0.09	26.78	0.45	10.19	5.83	0.20	99.40	49.1	1.1	286	1138
T873-79	92	ilmenitite	56.57	0.15	26.37	0.63	8.60	6.40	0.26	99.81	42.6	1.5		
T873-99	86	ilmenitite	56.10	0.11	26.99	0.60	9.18	5.92	0.26	99.71	46.1	1.5	283	1131
T873-101	17	opx-norite	56.38	0.06	26.81	0.40	9.29	5.24	0.79	99.23	49.5	4.8	341	1135
T873-125	8	opx-norite	56.98	0.06	26.73	0.34	9.03	5.33	1.02	99.66	48.4	6.1	461	1331
T873-133	73	opx-ilmenitite	56.06	0.10	26.99	0.38	9.31	5.47	0.45	99.14	48.5	2.7	336	1518
T873-146	64	norite	56.37	0.09	27.02	0.27	9.27	5.26	0.84	99.39	49.3	5.1	394	1193
T873-157	6	Allard anorthosite	56.79	0.06	26.11	0.70	8.98	5.41	1.04	99.64	47.8	6.2	275	1111
T873-166	5	Allard anorthosite	56.90	0.06	26.61	0.41	9.02	5.37	0.84	99.39	48.1	5.1	367	1125
T873-186	71	ilmenitite	55.90	0.10	27.18	0.32	9.49	5.30	0.67	99.12	49.7	4.0	319	1201
T873-190	5	Allard anorthosite	56.69	0.08	26.57	0.39	9.20	5.16	0.94	99.15	49.6	5.7	398	1165
T873-194	91	ilmenitite	56.39	0.13	27.15	0.37	9.31	5.87	0.22	99.71	46.7	1.3	331	1181
T873-202	87	ilmenitite	56.08	0.10	27.13	0.36	9.23	5.87	0.19	99.22	46.5	1.1	307	1324
T873-220	87	ilmenitite	56.02	0.10	27.00	0.33	9.21	5.81	0.19	98.99	46.7	1.1	313	1291
T873-242	90	ilmenitite	55.99	0.12	26.98	0.37	9.36	5.93	0.14	99.17	46.6	0.8		
T873-259	92	ilmenitite	56.02	0.14	26.81	0.42	9.77	5.96	0.14	99.56	47.5	0.8		
T873-268	57	opx-norite	55.89	0.10	27.46	0.25	9.59	5.65	0.25	99.40	48.4	1.5	270	1264
T873-283	91	ilmenitite	56.14	0.14	26.90	0.41	9.24	6.06	0.07	99.20	45.7	0.4		
T873-291	86	opx-ilmenitite	56.67	0.10	27.15	0.36	9.20	5.97	0.08	99.67	46.0	0.5		
T873-296	93	ilmenitite	56.24	0.11	27.11	0.35	9.63	5.93	0.07	99.80	47.3	0.4		
T873-301	88	opx-ilmenitite	56.20	0.10	27.30	0.37	9.43	5.86	0.06	99.49	47.1	0.4	246	1366
T873-316	3	Allard anorthosite	56.45	0.04	26.84	0.29	8.52	5.43	1.04	98.91	46.4	6.3	194	1148
T873-320	76	opx-ilmenitite	57.00	0.06	26.71	0.32	8.75	6.01	0.31	99.36	44.6	1.8	198	1163
T873-321	38	opx-norite	57.96	0.05	25.74	0.55	8.11	5.93	0.52	99.15	43.0	3.2	101	1056
T873-322	4	HSP anorthosite	56.74	0.03	26.83	0.22	9.09	5.58	0.78	99.30	47.4	4.6	246	1139
T875-25	93	ilmenitite	57.16	0.11	25.73	0.55	8.33	6.44	0.18	99.27	41.7	1.1		
T875-35	86	ilmenitite	56.28	0.10	27.17	0.26	9.25	5.88	0.17	99.45	46.5	1.0	278	1204
T875-66	16	norite	56.90	0.07	26.92	0.29	9.28	5.25	0.83	99.62	49.4	5.0	346	1203
T875-79	89	ilmenitite	56.48	0.12	27.03	0.48	9.17	6.02	0.13	99.61	45.7	0.8	234	851
T875-91	0	Allard anorthosite	56.89	0.07	26.74	0.40	9.33	4.95	1.01	99.52	51.0	6.2	386	1151
T875-96	86	ilmenitite	56.02	0.09	27.52	0.36	9.67	5.68	0.19	99.87	48.5	1.1	181	1174
T875-106	91	ilmenitite	56.02	0.12	27.22	0.38	9.45	5.81	0.09	99.44	47.3	0.5	184	1184
T875-116	79	ilmenitite	56.40	0.08	27.05	0.32	9.35	5.64	0.38	99.39	47.8	2.3	251	1045
T875-140	0	HSP anorthosite	56.91	0.04	26.63	0.46	8.52	5.67	0.95	99.54	45.4	5.7	437	1026
T875-150	0	HSP anorthosite	57.01	0.03	26.61	0.30	8.69	5.67	0.89	99.33	45.9	5.3	284	1000
T875-165	0	HSP anorthosite	57.30	0.03	26.63	0.28	8.70	5.67	1.04	99.76	45.9	6.1	315	1135
N10-6	88	ilmenitite	55.47	0.12	27.33	0.36	9.66	5.52	0.27	99.08	49.2	1.6	300	1280
N10-15	79	ilmenitite	55.69	0.11	27.66	0.32	9.84	5.30	0.43	99.60	50.6	2.6	280	1293
N10-24	91	ilmenitite	55.87	0.11	27.35	0.31	9.67	5.62	0.25	99.46	48.7	1.5	283	1262
N10-33	91	ilmenitite	55.51	0.13	27.20	0.39	10.09	5.78	0.13	99.55	49.1	0.7	276	1177
N10-42	84	ilmenitite	55.77	0.12	27.02	0.48	9.54	5.78	0.27	99.39	47.7	1.6		
N10-52	91	ilmenitite	55.62	0.12	27.07	0.31	9.69	5.78	0.14	99.01	48.1	0.8	250	1187
N10-54	2	Allard anorthosite	56.97	0.09	26.74	0.54	8.10	5.76	0.97	99.62	43.7	5.9	310	1124
N10-60	90	ilmenitite	55.08	0.12	26.77	0.53	10.14	5.84	0.21	99.11	49.0	1.2		
N10-67	93	ilmenitite	55.72	0.11	26.75	0.34	9.88	5.98	0.13	99.31	47.7	0.7	220	1301
N10-72	89	ilmenitite	56.46	0.10	27.36	0.28	9.48	5.84	0.11	99.97	47.3	0.6	269	1255
N10-75	0	HSP anorthosite	56.76	0.05	26.76	0.31	9.51	5.68	0.77	99.94	48.1	4.4	250	1212
N10-106	0	HSP anorthosite	55.90	0.03	26.42	0.24	10.01	5.76	0.65	99.07	49.0	3.6	213	1164
N10-152	0	HSP anorthosite	56.81	0.03	26.79	0.24	9.41	5.57	0.63	99.53	48.3	3.7	237	1055
TL05	0	HSP anorthosite	56.39	0.04	26.89	0.33	9.16	5.57	0.72	99.14	47.6	4.3	244	1181
TL09	0	HSP anorthosite	56.70	0.04	26.62	0.38	8.62	5.44	1.18	99.28	46.7	7.1	262	986
TL16	0	HSP anorthosite	56.58	0.05	26.66	0.39	8.75	5.58	1.06	99.28	46.4	6.3	298	1167
TL19	5	opx-norite	56.30	0.05	27.02	0.51	9.43	5.29	0.84	99.60	49.6	5.0	348	1060
TL20	2	opx-norite	56.15	0.05	26.94	0.53	9.26	5.29	0.93	99.43	49.2	5.6	377	1000
TL21	0	HSP anorthosite	56.42	0.05	26.78	0.23	9.41	5.59	0.66	99.18	48.2	3.9	213	962
TL22	0	HSP anorthosite	56.58	0.03	26.90	0.31	9.20	5.54	0.70	99.33	47.9	4.2	235	1083
TL23	0	HSP anorthosite	56.76	0.03	27.03	0.25	9.32	5.52	0.62	99.59	48.3	3.7	206	1027
TL24	0	HSP anorthosite	56.94	0.03	26.78	0.24	9.14	5.55	0.67	99.41	47.6	4.0	196	1121
TL25	0	HSP anorthosite	56.82	0.03	26.70	0.27	9.13	5.62	0.64	99.26	47.3	3.8	272	1055
TL26	0	HSP anorthosite	56.90	0.03	26.87	0.27	9.01	5.65	0.70	99.51	46.8	4.2	221	1098
TL31	0	HSP anorthosite	56.73	0.05	26.83	0.27	9.25	5.49	0.62	99.29	48.2	3.7	230	1182
TL35	10	HSP anorthosite	57.02	0.21	26.68	0.27	9.09	5.50	0.81	99.77	47.7	4.8	391	1142
TL36	4	opx-norite	56.57	0.04	26.84	0.38	9.15	5.56	0.78	99.61	47.6	4.6	335	1121
TL37	0	HSP anorthosite	56.92	0.07	26.45	0.30	8.93	5.56	0.74	99.06	47.0	4.4	287	1134

An = 100 [Ca/(Ca+Na)]; Or = 100 [K/(Ca+Na+K)]; Sr and Ba in ppm

Table3
Click here to download Table: Table3.xls

Table 3
Microprobe analyses of aluminous spinel from the Allard Lake ilmenite deposit

Sample	n	Ilm prop	Rock type	TiO_2	Al_2O_3	FeO	MgO	MnO	Cr_2O_3	ZnO	V_2O_3	Total	Xherc	Xspinel	Xgal	Xgah
T873-68	12	95	ilmenitite	0.01	62.87	16.67	17.10	0.06	0.71	1.48	0.05	98.94	0.344	0.628	0.001	0.027
T873-133	11	73	opx-ilmenitite	0.04	60.02	17.99	15.39	0.05	3.63	2.02	0.07	99.21	0.381	0.580	0.001	0.038
T873-268	11	57	opx-norite	0.04	61.42	20.07	15.44	0.06	0.92	1.26	0.07	99.28	0.412	0.564	0.001	0.023
T873-291	14	86	opx-ilmenitite	0.02	62.59	18.52	15.83	0.06	0.88	1.14	0.06	99.10	0.387	0.590	0.001	0.021
T873-296	84	93	ilmenitite	0.04	62.07	18.57	16.32	0.06	1.05	1.12	0.06	99.29	0.381	0.597	0.001	0.020

Xherc, Xspinel, Xgal and Xgah are molar fractions of hercynite ($FeAl_2O_4$), spinel ($MgAl_2O_4$), galaxite ($MnAl_2O_4$) and gahnite ($ZnAl_2O_4$) respectively; n is the number of microprobe analyses.

Table4
Click here to download Table: Table4.xls

Table 4
Microprobe analyses of orthopyroxene, clinopyroxene and sapphirine from the Allard Lake ilmenite deposit and the host Havre-Saint-Pierre anorthosite

Sample	n	Ilm prop	Rock type	SiO_2	TiO_2	Al_2O_3	FeO	MnO	MgO	CaO	Na_2O	Total	Mg#	En	Fs	Wo
Orthopyroxene																
T873-68	15	95	ilmenitite	50.39	0.15	7.77	14.85	0.18	26.04	0.03	0.03	99.44	75.8	75.7	24.2	0.1
T873-101	22	17	opx-norite	52.61	0.14	1.53	20.47	0.33	23.28	0.72	0.02	99.10	67.0	66.0	32.5	1.5
T873-125	21	8	opx-norite	52.88	0.13	1.81	19.72	0.31	23.89	0.69	0.02	99.45	68.4	67.4	31.2	1.4
T873-133	14	73	opx-ilmenitite	52.56	0.17	3.09	16.98	0.24	25.73	0.46	0.02	99.25	73.0	72.3	26.8	0.9
T873-190	21	5	Allard anorthosite	51.18	0.13	2.87	22.71	0.44	21.74	0.29	0.02	99.38	63.0	62.7	36.7	0.6
T873-268	10	57	opx-norite	49.02	0.16	9.08	16.94	0.19	23.99	0.05	0.03	99.46	71.6	71.5	28.3	0.1
T873-291	17	86	opx-ilmenitite	49.94	0.15	8.36	16.13	0.18	24.80	0.06	0.01	99.63	73.3	73.2	26.7	0.1
T873-296	20	93	ilmenitite	49.82	0.18	8.46	15.33	0.17	25.45	0.09	0.02	99.52	74.7	74.6	25.2	0.2
T875-87	12	95	ilmenitite	50.42	0.20	7.62	15.84	0.19	26.01	0.14	0.02	100.44	74.5	74.3	25.4	0.3
N10-75	10	0	HSP anorthosite	53.01	0.14	1.50	21.12	0.59	23.40	0.57	0.01	100.34	66.4	65.6	33.2	1.1
TL19	13	5	opx-norite	53.08	0.22	1.66	19.92	0.35	24.06	0.71	0.02	100.02	68.3	67.3	31.3	1.4
TL20	19	2	opx-norite	52.60	0.17	1.48	21.16	0.39	22.98	0.59	0.02	99.39	65.9	65.1	33.7	1.2
TL31	10	0	HSP anorthosite	51.61	0.21	1.54	24.83	0.84	20.14	0.54	0.02	99.73	59.1	58.4	40.4	1.1
TL36	25	4	opx-norite	52.65	0.15	1.60	20.73	0.32	23.14	0.66	0.02	99.27	66.6	65.6	33.0	1.4
Clinopyroxene																
T873-166	21	5	Allard anorthosite	50.80	0.58	2.81	8.71	0.20	13.22	22.55	0.47	99.34	73.0	38.5	14.2	47.2
N10-75	6	0	HSP anorthosite	52.21	0.29	2.10	7.36	0.23	14.28	23.47	0.35	100.29	77.6	40.5	11.7	47.8
N10-152	10	0	HSP anorthosite	51.72	0.33	2.30	8.51	0.33	13.27	22.98	0.47	99.91	73.5	38.4	13.8	47.8
TL20	12	2	opx-norite	51.17	0.57	2.83	8.71	0.18	13.56	21.89	0.47	99.38	73.5	39.7	14.3	46.0
TL31	20	0	HSP anorthosite	51.28	0.44	2.87	8.69	0.26	13.12	22.50	0.49	99.65	72.9	38.4	14.3	47.3
Sapphirine																
T873-68	4	95	ilmenitite	12.70	0.06	59.68	9.17	0.07	16.14	0.01	0.01	97.89				
T873-268	18	57	opx-norite	11.96	0.09	61.62	8.60	0.05	15.90	0.01	0.00	98.23				

Mg# =100 [Mg/(Mg+Fe)]; En = 100 [Mg/(Mg+Fe+Ca)]; Fs = 100 [Fe/(Mg+Fe+Ca)]; Wo = 100 [Ca/(Mg+Fe+Ca)]